

---

Doctoral Dissertations

Student Theses and Dissertations

---

Summer 2018

## Investigation of additively manufactured polymer and transparent polymer composites

Gregory Taylor

Follow this and additional works at: [https://scholarsmine.mst.edu/doctoral\\_dissertations](https://scholarsmine.mst.edu/doctoral_dissertations)



Part of the [Aerospace Engineering Commons](#)

Department: Mechanical and Aerospace Engineering

---

### Recommended Citation

Taylor, Gregory, "Investigation of additively manufactured polymer and transparent polymer composites" (2018). *Doctoral Dissertations*. 2899.

[https://scholarsmine.mst.edu/doctoral\\_dissertations/2899](https://scholarsmine.mst.edu/doctoral_dissertations/2899)

This thesis is brought to you by Scholars' Mine, a service of the Missouri S&T Library and Learning Resources. This work is protected by U. S. Copyright Law. Unauthorized use including reproduction for redistribution requires the permission of the copyright holder. For more information, please contact [scholarsmine@mst.edu](mailto:scholarsmine@mst.edu).

INVESTIGATION OF ADDITIVELY MANUFACTURED POLYMER AND  
TRANSPARENT POLYMER COMPOSITES

by

GREGORY ALLEN TAYLOR

A DISSERTATION

Presented to the Faculty of the Graduate School of the  
MISSOURI UNIVERSITY OF SCIENCE AND TECHNOLOGY

In Partial Fulfillment of the Requirements for the Degree

DOCTOR OF PHILOSOPHY

in

AEROSPACE ENGINEERING

2018

Approved by:

K. Chandrashekhara, Advisor

E. Kinzel

M. Leu

T. Schuman

X. Yang

© 2018

Gregory Allen Taylor

All Rights Reserved

## **PUBLICATION DISSERTATION OPTION**

This dissertation has been prepared in the form of three papers for publication as follows:

Paper I: Flexural Behavior of Additively Manufactured Ultem 1010: Experiment and Simulation (Pages 6-32). This paper has been published in Rapid Prototyping Journal, 2018.

Paper II: Fracture Toughness of Additively Manufactured Ultem 1010 (Pages 33-49). The paper is intended for submission to Virtual and Physical Prototyping.

Paper III: Mechanical and Optical Behavior of a Continuous Glass Fiber-Reinforced Transparent Composite (Pages 50-64). The paper is intended for submission to Applied Composite Materials.

## ABSTRACT

The objective of this study is an investigation of both the characterization of fused deposition modeling (FDM) of polymer thermoplastics and the manufacture of glass-reinforced transparent composites. The flexural behavior and fracture toughness of FDM parts are critical for the evaluation and optimization of both material and process. This study focuses on the performance of FDM Ultem 1010 specimens intended to be used as composite tooling due to the material's high heat resistance. A three-point bend test is performed for flexure properties while a single edge notch bend test is performed for fracture toughness. For each of the tests, the build parameters are investigated through a full-factorial design of experiments with results including flexure properties and fracture toughness properties. For flexure tests, additional tests are performed at elevated temperatures and on sparse coupons for the validation of a finite element simulation. Thermo-mechanical finite element simulation results are in good agreement with experimental findings. Transparent composite panels composed of an S-glass fabric and epoxy resin are manufactured and evaluated to introduce new materials for armor applications. The epoxy resin is synthesized from Epon 826, Epalloy 5200, and Hexahydrophthalic Anhydride. To improve optical clarity, the fibers and resin are first manufactured in small samples to incrementally narrow the refractive index of the resin until matching with the glass fiber refractive index. Upon successful matching of refractive indices, a large batch of resin is synthesized to manufacture the transparent composite panels. Composite panels are manufactured with the cost-effective vacuum assisted resin transfer molding to ensure optical transparency. Currently, the proposed performance evaluation of the composite panels will involve tensile and flexure tests.

## ACKNOWLEDGEMENTS

I express my deepest gratitude to my academic advisor, Dr. K Chandrashekhara, whose guidance and support helped me throughout both my master's and Ph.D. degree. His constructive suggestions have been invaluable during the course of my graduate research. I express thanks to the members of my advisory committee E. Kinzel, M. Leu, T. Schuman, X. Yang for both their time and advice in the review of this dissertation. I am grateful for the members of the Composite Research group, especially X. Wang, S. Anandan, and D. Murphy who worked with me during my research. I am also thankful for Timothy Schniepp and Ross Jones (Stratasys) and The Center for Aerospace Manufacturing Technologies (CAMT) for their advice and financial support. Lastly, I also thank my family for all their love, encouragement, and support throughout my time at Missouri S&T.

## TABLE OF CONTENTS

	Page
PUBLICATION DISSERTATION OPTION .....	iii
ABSTRACT.....	iv
ACKNOWLEDGEMENTS .....	v
LIST OF ILLUSTRATIONS .....	ix
LIST OF TABLES .....	xi
 SECTION	
1. INTRODUCTION.....	1
2. SCOPE AND OBJECTIVES.....	4
 PAPER	
I. FLEXURAL BEHAVIOR OF ADDITIVELY MANUFACTURED ULTEM 1010: EXPERIMENT AND SIMULATION .....	6
ABSTRACT .....	6
1. INTRODUCTION .....	7
2. EXPERIMENTAL METHODOLOGY .....	10
2.1. SPECIFICATIONS AND DESIGN OF EXPERIMENTS FOR FLEXURE TESTING .....	11
2.2. SPECIFICATIONS FOR ULTEM 1010 TENSILE TESTING.....	13
2.3. FABRICATION OF ULTEM 1010 SPECIMENS WITH THE FDM PROCESS .....	14
2.4. TESTING PROCEDURE .....	15
3. MODELING AND SIMULATION .....	16
4. RESULTS AND DISCUSSION.....	19

4.1. SOLID SAMPLE FLEXURE RESULTS FOR VARYING BUILD PARAMETERS .....	19
4.2. SOLID SAMPLE FLEXURE RESULTS AT ELEVATED TEMPERATURES.....	22
4.3. SPARSE SAMPLE FLEXURE RESULTS FOR SIMULATION VALIDATION .....	23
4.4. SOLID SAMPLE TENSILE TEST RESULTS .....	25
4.5. SIMULATION RESULTS.....	25
5. CONCLUSIONS .....	29
ACKNOWLEDGEMENTS .....	29
REFERENCES .....	30
II. FRACTURE TOUGHNESS OF ADDITIVELY MANUFACTURED ULTEM 1010 .....	33
ABSTRACT .....	33
1. INTRODUCTION .....	34
2. EXPERIMENTAL METHODOLOGY .....	36
2.1. SPECIFICATIONS AND DESIGN OF EXPERIMENTS FOR FRACTURE TOUGHNESS TESTING.....	36
2.2. FABRICATION OF ULTEM 1010 SPECIMENS WITH THE FDM PROCESS.....	38
2.3. FRACTURE TOUGHNESS TESTING PROCEDURE.....	39
3. RESULTS AND DISCUSSION.....	42
3.1. FRACTURE TOUGHNESS RESULTS .....	42
3.2. DESIGN OF EXPERIMENTS RESULTS .....	43
3.3. MICROSTRUCTURE EVALUATION .....	44
4. CONCLUSIONS .....	47

ACKNOWLEDGEMENTS .....	47
REFERENCES .....	47
III. MECHANICAL AND OPTICAL BEHAVIOR OF A CONTINUOUS GLASS FIBER-REINFORCED TRANSPARENT COMPOSITE .....	50
ABSTRACT .....	50
1. INTRODUCTION .....	50
2. MATERIALS .....	52
2.1. FIBER REINFORCEMENT SELECTION .....	52
2.2. EPOXY SELECTION AND SYNTHESIS.....	53
3. MANUFACTURING .....	55
4. EXPERIMENTAL METHODOLOGY .....	58
4.1. TENSION TEST SPECIFICATIONS .....	58
4.2. FLEXURE TEST SPECIFICATION.....	59
5. RESULTS .....	60
5.1. TENSION TEST RESULTS .....	60
5.2. FLEXURE TEST RESULTS .....	61
6. CONCLUSIONS .....	62
REFERENCES .....	63
SECTION	
3. CONCLUSIONS .....	65
VITA.....	67

## LIST OF ILLUSTRATIONS

PAPER I	Page
Figure 1. Flexure coupon (blue) dimensions and setup for three-point (orange) bending test.....	11
Figure 2. Build orientation for flexure samples .....	13
Figure 3. Tensile specimen dimensions (in. [mm]) with a gauge section width of 0.50 in. (13 mm) and thickness of 0.28 in. (7 mm).....	14
Figure 4. Flexure experimental setup.....	16
Figure 5. Modeling of flexure coupon .....	17
Figure 6. Coupon designs for compression tests .....	18
Figure 7. Simulation model for flexure test .....	19
Figure 8. Ultem 1010 modulus for varying build orientation and raster angle.....	20
Figure 9. Ultem 1010 yield strength for varying build orientation and raster angle .....	21
Figure 10. Elevated temperature (°C) stress-strain curves for solid flexure Ultem 1010 samples .....	23
Figure 11. Reduction of modulus and yield strength with increased temperature for solid Ultem 1010 flexure samples.....	24
Figure 12. Flexure modulus and yield strength of XYZ 0°/90° Ultem 1010 coupons .....	24
Figure 13. Compression vs. tension stress-strain results .....	26
Figure 14. Comparison of solid flexure test between experiment and simulation.....	26
Figure 15. Plastic strain distribution of FDM part during flexure test.....	27
Figure 16. Modeling of sparse XYZ 0°/90° FDM parts with: (a) 2.54 mm air gap, (b) 5.08 mm air gap.....	27
Figure 17. Stress (von Mises) distribution during flexure test (2.54 mm air gap) and comparison of sparse flexure test between experiment and simulation .....	28

Figure 18. Stress (von Mises) distribution during flexure test (5.08 mm air gap) and comparison of sparse flexure test between experiment and simulation .....	28
--	----

## PAPER II

Figure 1. Build orientation .....	39
Figure 2. Specimen dimensions for fracture toughness test .....	40
Figure 3. Test setup for the SENB fracture toughness test .....	41
Figure 4. (a) Partial fracture of an Ultem 1010 sample, (b) Complete fracture of an Ultem 1010 sample .....	42
Figure 5. Average KIQ of varying build orientation and raster angles for Ultem 1010 samples .....	43
Figure 6. (a) Samples with all 0° rasters, (b) Samples with all 90° rasters .....	46
Figure 7. (a) Samples with 0°/90° rasters, (b) Samples with 45°/-45° rasters .....	46

## PAPER III

Figure 1. Resin system test sample with S-glass fibers .....	54
Figure 2. VARTM process schematic for transparent composites .....	56
Figure 3. VARTM layup before infusion .....	57
Figure 4. Transparent composite cure cycle .....	58
Figure 5. Tension test setup for transparent composites .....	59
Figure 6. Four-point flexure test setup for transparent composites .....	60
Figure 7. Tensile stress-strain curves for the transparent composite .....	61
Figure 8. Flexural stress-strain curves for the transparent composite .....	62

## LIST OF TABLES

PAPER I	Page
Table 1. Full-factorial design of experiments for solid coupon flexure testing.....	13
Table 2. Compression and tension properties used in finite element model .....	18
Table 3. DOE analysis: modulus effects for different build parameters during flexure testing.....	22
Table 4. DOE analysis: yield strength effects for different build parameters during flexure testing .....	22
PAPER III	
Table 1. Full-factorial design of experiments .....	37
Table 2. Analysis of variance.....	45
Table 3. Build parameter effects table .....	45
PAPER III	
Table 1. Refractive indices of fiber and resin .....	53
Table 2. Resin system .....	55

## **SECTION**

### **1. INTRODUCTION**

Additive manufacturing is a process in which layers of material are formed and added to additional layers to create a three-dimensional part. One of the processes for additive manufacturing is fused deposition modeling (FDM) which involves the extrusion of plastics through a nozzle to form the layers of the part. Typical materials for FDM include thermoplastics such as acrylonitrile butadiene styrene (ABS), Nylon, polylactic acid (PLA), Ultem 9085, Ultem 1010, and polycarbonate (PC). FDM machines offer a variety of build parameters including build direction, raster angle, raster width, wall thickness, and cap thickness, and different configurations of the build parameters can alter the properties of the parts. Both design of experiments (DOE) and finite element analysis (FEA) offer the capability to understand the effects of the build parameters.

Design of experiments (DOE) is a statistical approach to understanding how different conditions vary the outcome of an experiment. Typically, a group of factors is selected that possibly affects an intended response. Implementing a DOE to examine how build parameters (factors) possibly affect one or more responses (mechanical properties) allows a better understanding of the behavior of these build parameters.

FEA has been widely used in modeling of many structural applications. Additive manufacturing introduces new complexities into an FEA including orthotropic behavior, optimization of sparse-build parts, and geometric complexity. While

preliminary work using FEA has been undertaken to understand these complexities, the effects of build parameters is a problem that has not been fully characterized.

In structural applications, the most common transparent material utilized today is glass. However, glass is not desired for applications in which weight can heavily impact the performance of a structure. These applications include aerospace windows and canopies, armored vehicle windows, visors, and buildings. If a lightweight, high strength alternative such as transparent composites can be developed, these structures can reduce weight while maintaining or improving the overall strength of the transparent material. To achieve this, the transparent composite needs to have continuous glass fiber reinforcement with a strong polymer matrix. To ensure transparency of a heterogeneous composite material, both glass fiber and polymer matrix need have matching refractive indices.

In the current study, Ultem 1010 and the FDM process are investigated for the effects of changing build parameters for solid-build and sparse-build specimens. Additionally, additively manufactured Ultem 1010 specimens are tested for flexural and tensile properties at elevated temperatures. Build parameters including building direction, raster angle, and air gap are investigated utilizing design of experiments (DOE) for their effects on the flexural properties of an Ultem 1010 part. A finite element simulation was developed to help evaluate sparse-build coupons with varying build parameters. Due to the desire to implement additively manufactured Ultem 1010 samples into structural applications in the future, the fracture toughness is studied for varying build parameters. Also in the present work, transparent composites are manufactured using the vacuum assisted resin transfer molding (VARTM) process. An S-glass fiber fabric with an

epoxy-based resin is used to manufacture the transparent composites. Manufactured panels are subjected to mechanical testing to determine both tensile and flexural properties of the transparent composite.

## 2. SCOPE AND OBJECTIVES

This dissertation is comprised of three papers dealing with the following problems. The first paper is titled, “Flexural Behavior of Additively Manufactured Ultem 1010: Experiment and Simulation.” In this paper, the flexural performance of solid and sparse Ultem 1010 specimens is evaluated using DOE. The Ultem 1010 specimens are manufactured using FDM and tested for flexural properties. Experimental results are tabulated based on varying the build parameters of the FDM specimens. A full-factorial DOE is utilized to understand how the different build parameters affect the flexural properties. A three-dimensional nonlinear finite element model is built to simulate the flexural behavior of the FDM parts. The model is compared with the experimental results and found to be in good agreement.

The second paper is titled, “Fracture Toughness of Additively Manufactured Ultem 1010.” In this paper, additively manufactured Ultem 1010 specimens are investigated for fracture toughness. Specimens are first manufactured utilizing the FDM manufacturing process. Build direction and raster angle are varied to evaluate their effect on the critical stress intensity factor ( $K_{I0}$ ). A full-factorial DOE is performed to study how the build direction and raster angle affect the fracture toughness. The primary results include a relationship of the build parameters and fracture toughness of Ultem 1010.

The third paper is titled, “Mechanical and Optical Behavior of a Continuous Glass Fiber-Reinforced Transparent Composite.” This study evaluates the tensile and flexural performance of a continuous fiber transparent composite. An epoxy resin is synthesized to match the refractive index of S-glass fibers. Transparent composite panels are manufactured using the vacuum assisted resin transfer molding process. The composite is

tested for tension and flexure properties. The primary results include a working S-glass fiber/epoxy resin system for manufacturing transparent composites as well as mechanical properties of the composite.

**PAPER****I. FLEXURAL BEHAVIOR OF ADDITIVELY MANUFACTURED ULTEM 1010:  
EXPERIMENT AND SIMULATION**

Gregory Taylor, Xin Wang, Leah Mason, Ming Leu, and K. Chandrashekhara

Department of Mechanical and Aerospace Engineering

Intelligent Systems Center

Missouri University of Science and Technology, Rolla, MO 65409

Timothy Schniepp and Ross Jones

Stratasys Inc., Eden Prairie, MN 55344

**ABSTRACT**

Fused deposition modeling (FDM) process has become one of most widely used additive manufacturing methods. The process provides the capability of fabricating complicated shapes through the extrusion of plastics onto a print surface in a layer-by-layer structure to build three-dimensional parts. The flexural behavior of FDM parts are critical for the evaluation and optimization of both material and process. This study focuses on the performance of FDM solid and sparse-build Ultem 1010 specimens. Flexure tests (three-point bend) are performed on solid-build coupons with varying build orientation and raster angle. These parameters are investigated through a full-factorial design of experiments (DOE) to determine optimal build parameters. Air gap, raster width and contour width are held constant. A three-dimensional nonlinear finite element model is built to simulate the flexural behavior of the FDM parts. Experimental results

include flexure properties such as yield strength and modulus, as well as analysis of the effect of change in build parameters on material properties. The sparse-build FDM parts chosen from the experimental tests are simulated based on this developed model. Thermo-mechanical simulation results show that the finite element simulation and experimental tests are in good agreement. The simulation can be further extended to other complicated FDM parts. From the DOE study, sparse-build coupons with specific build parameters are fabricated and tested for the validation of a finite element simulation.

## **1. INTRODUCTION**

Additive manufacturing began as a process to build small-scale prototypes, but over the past decade, it has become a widely accepted and utilized method of manufacturing. While traditional fabrication techniques often require a considerable amount of subtractive machining, additive manufacturing eliminates a substantial portion of the subtractive manufacturing owing to its method of fabrication. Additive manufacturing takes a three-dimensional computer-aided design (CAD) model of a proposed part and builds each layer at a time, continually stacking additional layers until completion. This process allows for complex parts that are not typically able to be produced by traditional subtractive manufacturing techniques. Because this is a relatively new process, in comparison to the older subtractive techniques, the industry needs to develop approaches to optimally produce parts using this method. Owing to the automated manufacture and reduced material cost from the minimal waste of the process, additive manufacturing has been adopted widely in the manufacturing industry and has become a popular topic of research.

One of the common additive manufacturing processes commonly utilized is fused deposition modeling (FDM). This process extrudes a semi-liquid or liquid thermoplastic through a nozzle onto the build platform where the thermoplastic solidifies to form the layer and eventually the part. To accurately control the additive manufacturing, the CAD model is imported into the FDM machine in a stereolithography file format, and the FDM machine moves the nozzle and/or build platform to build the part. Complex parts are produced with the addition of support material to the finished part's component material. This support material provides the structure for overhangs or extensions beyond which the component material will not support itself.

Researchers have been studying the mechanical behavior of FDM specimens and the effects that build parameters have on their performance. Zaldivar *et al.* [1] studied how the selection of build orientation will vary the tensile properties, Poisson's ratio, and the coefficient of thermal expansion of Ultem 9085. Luzanin *et al.* [2] looked at the flexural properties of polylactic acid (PLA) through the influence of the layer thickness, deposition angle, and infill. Motaparti *et al.* [3] incorporated a design of experiments approach to study the effects of FDM build parameters on Ultem 9085. Taylor *et al.* [4] examined the effect of raster angle, air gap, and contour thickness on the compressive properties of Ultem 1010. Rayegani, *et al.* [5] implemented the group method of data handling (GMDH) to predict tensile strength of FDM produced parts varying in build orientation, raster angle, and air gap. Casavola *et al.* [6] used classical laminate theory typically seen in composite structures to describe the mechanical behavior of FDM parts. Li *et al.* [7] investigated the use of FDM material (specifically Ultem 9085) as a substitute for composite molds and simulated the composite manufacturing process

utilizing the molds. Researchers have also begun studying the effects of additives to the thermoplastic material for FDM manufacturing. Torrado *et al.* [8] and Weng *et al.* [9] have inserted additives into ABS material to analyze the altering of the mechanical properties.

Finite element analysis has been widely used in the modeling of additive manufacturing process and corresponding products. Ji and Zhou [10] used the finite element method to evaluate the temperature distribution during the fused deposition modeling process, and found that the greatest temperature gradient was located near the edges of parts. Gorski *et al.* [11] developed a finite element method to calculate the mechanical properties of FDM parts, and this model was verified by experimental results. Domingo-Espin *et al.* [12] built an effective finite element model based FDM part tension tests to optimize build parameters. This verified finite element modeling can predict the proper material orientation with greater tensile stress under varying loading conditions. Rezayat *et al.* [13] investigated the relationship between FDM parts' mechanical properties and building parameters using a finite element method and an experimental method, and provided an effective way to optimize the raster contour fill pattern. Garg and Bhattacharya [14] studied the failure behavior of FDM parts under tensile loading, and the finite element results showed that there is a brittle failure of  $0^\circ$  raster angle at the necking area. Villalpando *et al.* [15] developed an optimization method considering build time, material usage, surface quality, and other related parameters to assist design process. Jerez-Mesa *et al.* [16] used the finite element method to analyze the thermal behavior during additive manufacturing process. Sayre [17] investigated mechanical behavior of isotropic ABS parts and FDM ABS parts using finite element method and

concluded FDM parts are an appropriate tool for application. Liang [18] studied FDM application for microwave patch antenna employing finite element method. Mohamed *et al.* [19] provided a comprehensive review on the optimization of fused deposition modeling process and discussed finite element method on FDM. These literatures provide research background for current study.

In literature, the mechanical properties including tension and flexure, as well as experimental-based simulations of Ultem 1010, are limited. In the current study, investigations of the mechanical properties of Ultem 1010 are performed to study flexural behavior of Ultem 1010. Solid coupons with varying build parameters (build orientation and raster angle) were manufactured and evaluated with a full-factorial DOEs. Flexure tests at elevated temperatures up to 205°C (400°F) were also performed on Ultem 1010 solid coupons for one of the build parameter combinations. Two sets of sparse-build Ultem 1010 flexure coupons were also tested for a simulation validation. The simulation was developed to predict the flexure behavior of Ultem 1010 sparse-build coupons.

## **2. EXPERIMENTAL METHODOLOGY**

The experimental portion of this study consists of four experiments. First, solid sample flexure tests with varying build parameters are conducted to determine flexural modulus, yield strength and nonlinear stress–strain curves. Second, tension tests are conducted to determine tensile modulus, yield strength and nonlinear stress–strain curves for input into the finite element simulation. Third, elevated temperature tests on a solid flexure samples with a specified combination of build parameters to investigate the nonlinear behavior of the flexural properties as a function of temperature. Finally, sparse

sample flexure tests are performed as a case study validation to the finite element simulation.

## 2.1. SPECIFICATIONS AND DESIGN OF EXPERIMENTS FOR FLEXURE TESTING

Ultem 1010 flexure samples were fabricated according to ASTM D-790 Standard Test Methods for Flexural Properties of Unreinforced and Reinforced Plastics and Electrical Insulating Materials [20]. All flexural samples were manufactured with dimensions of 127 mm x 25.4 mm x 6.35 mm (5 in. x 1 in. x 0.25 in.) as shown in Figure 1.

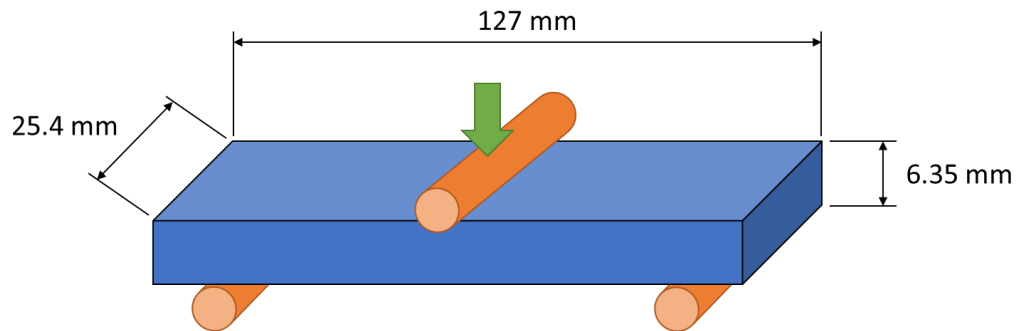


Figure 1. Flexure coupon (blue) dimensions and setup for three-point (orange) bending test

Solid samples for varying build parameters (build orientation and raster angle) followed a full-factorial DOE (Table 1). In this DOE, build orientation and raster angle are the independent variables called “factors” with several levels of variation. Build orientation has three levels including XYZ, ZXY and XZY. These terms are taken directly from Stratasys [21] and ISO/ASTM52921-13 Standard Terminology for

Additive Manufacturing-Coordinate Systems and Test Methodologies [22] and are typically used for their additive manufacturing test procedures. The difference between the build orientations is shown in Figure 2. The raster angle had two levels including  $0^\circ/90^\circ$  and  $45^\circ/_45^\circ$ . The raster angles are measured as the angle of the interior rasters with respect to the outside contours of the solid and sparse samples. Raster width, contour width and air gap were held constant at 0.508, 0.508 and 0 mm, respectively. With three levels of build orientation and two levels of raster angle, the total number of build combination was six, and with five replications at each build combination, a total of 30 samples were manufactured.

Upon completion of the initial experiment involving the variation in solid sample build parameters. The XYZ  $0^\circ/90^\circ$  build combination was used as the basis for the elevated temperature testing. The XYZ  $0^\circ/90^\circ$  build combination was chosen for the elevated temperature tests due to the ZXY and XZY build combinations' properties being almost entirely dependent on the contour properties (critical location for flexural failure), which is unchanged, except orientation, in all cases. The XYZ  $0^\circ/90^\circ$  coupons were tested at six temperatures including 25, 80, 120, 150, 177, 205°C (77, 180, 250, 300, 350, 400°F). These temperatures were chosen due to their relationship to composite manufacturing (Boeing recommendation). With six total temperatures and five replications at each temperature, a total of 30 additional samples were manufactured.

The final flexure tests were performed on sparse samples with the same XYZ  $0^\circ/90^\circ$  build combination, however the sparse samples have 2.54 mm (0.1 in.) and 5.08 mm (0.2 in.) air gaps. All other parameters remained the same as the XYZ  $0^\circ/90^\circ$  solid

samples. With two total air gaps and five replications at each air gap, a total of ten sparse samples were manufactured.

Table 1. Full-factorial design of experiments for solid coupon flexure testing

Factors	Levels		
	-1	0	1
Build Orientation	XYZ	ZXY	XZY
Raster Angle	0°/90°	-	45°/-45°
<b>Constants</b>			
Raster Width	0.508 mm (0.02 in.)		
Contour Width	0.508 mm (0.02 in.)		
Air Gap	None for Solid Samples		

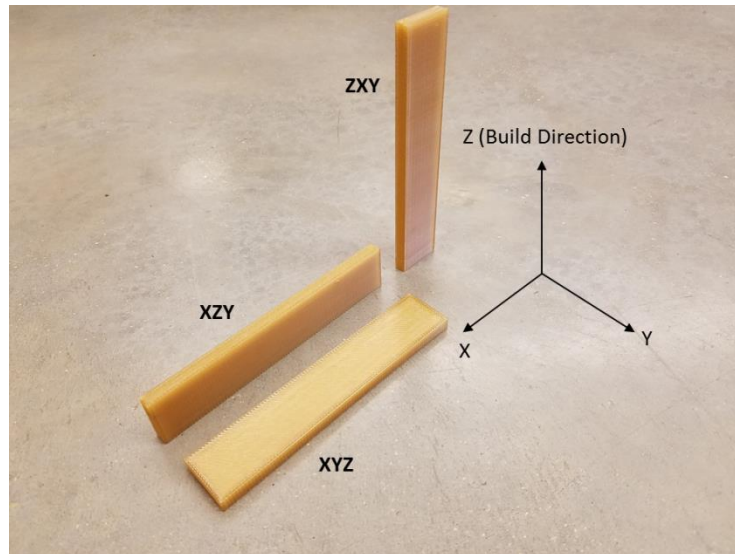


Figure 2. Build orientation for flexure samples

## 2.2. SPECIFICATIONS FOR ULTEM 1010 TENSILE TESTING

Ultem 1010 tensile samples were fabricated according to ASTM D-638-14 Standard Test Method for Tensile Properties of Plastics (22). All tensile “dog-bone”

samples were manufactured with dimensions for Type I geometry as shown in Figure 3. Only solid samples with the XYZ 0°/90° build combination were fabricated and tested to match the tensile properties observed in the flexure coupons for the simulation case-study. A total of five samples were tested and the tensile modulus and yield strength were measured.

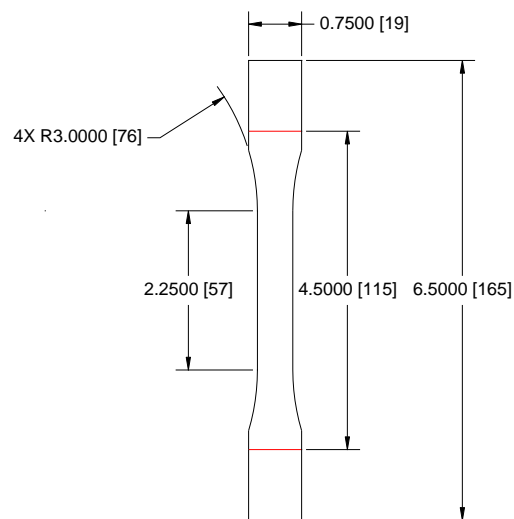


Figure 3. Tensile specimen dimensions (in. [mm]) with a gauge section width of 0.50 in. (13 mm) and thickness of 0.28 in. (7 mm)

### 2.3. FABRICATION OF ULTEM 1010 SPECIMENS WITH THE FDM PROCESS

For the three experiments, all the FDM parts were fabricated with Ultem 1010 using the Stratasys Fortus 400mc machine at Missouri University of Science and Technology.

The process for the fabrication of these FDM parts involves the following process:

1. Pre-processing: Test coupons were modeled in three dimensions using CAD software with dimensions of 127 mm x 25.4 mm x 6.35 mm. Models are exported as a Stereo Lithography (STL) file to Stratasys Insight 9.1 software.

The Insight software creates the build toolpath for the Fortus machine and specifies build parameters of the FDM parts. The STL file is then provided to the FDM machine for fabrication of the flexure parts.

2. Fabrication: The Fortus 400mc machine then fabricated the FDM parts through the extrusion of Ultem 1010 filament via a heated nozzle in a layer-by-layer manner until completion. The Ultem 1010 support material (Polyethersulfone) was used as the breakaway support material.
3. Post-processing: After fabrication, the flexure coupons are separated mechanically from the support structure (required for FDM manufacturing) and marked for experimental testing.

#### **2.4. TESTING PROCEDURE**

The experimental portion of this study consisted of four primary experiments. The first experiment tested solid sample flexure coupons with varying build parameters. The second test examined flexure properties at elevated temperature with a specified combination of build parameters derived from the first test. The third test found flexure properties of sparse coupons with a specified combination of build parameters as a case-study validation to supplement the finite element simulation. The final test found tensile properties of solid coupons with a specified combination of build parameters to match the tensile loading seen in the flexure samples for the simulation.

Flexure tests were performed according to ASTM D-790 Standard Test Methods for Flexural Properties of Unreinforced and Reinforced Plastics and Electrical Insulating Materials. All 70 samples were tested on an Instron 5985 universal testing machine. The

thirty elevated temperature samples were tested in the attached temperature chamber on the Instron 5985. Load and deflection were recorded, and calculations were completed after testing for flexural stress and yield strength. The experimental setup is shown in Figure 4 for a solid build coupon.

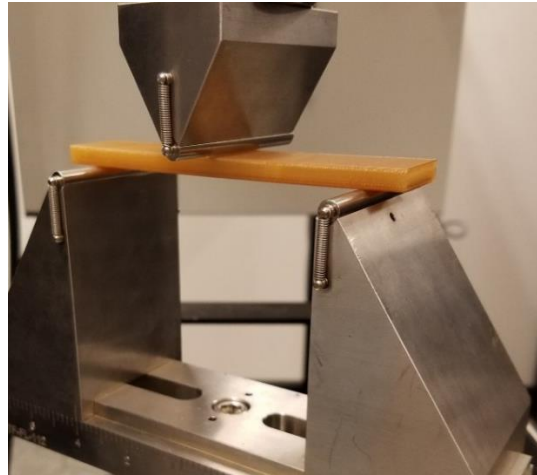


Figure 4. Flexure experimental setup

Tensile tests were performed according to ASTM D-638-14 Standard Test Method for Tensile Properties of Plastics. The five samples were tested on an Instron 5985 universal testing machine. Strain rate for testing was 5 mm/min. Load and deflection were recorded, and calculations were completed after testing for tensile stress and yield strength.

### 3. MODELING AND SIMULATION

In the current flexure simulation, the FDM parts were modeled with same dimensions as manufactured parts (127 mm x 25.4 mm x 6.35 mm). The top puncher was

modeled as rigid to deform the FDM part, and bottom supports were modeled as boundary condition fixing in deformation direction. According to the flexure experimental test, both solid and sparse built FDM specimens were built in the finite element model. Following the experimental procedure, the simulated flexure speed is 0.042 mm/s (0.1 in./min) with compressive displacement 15.2 mm (0.6 in.), and the simulated compressing time is 350 s (Figure 5). The load and displacement of the top puncher was monitored for comparison with experimental data.

Due to the characteristics of a flexure test, the top of the testing coupon is under compression while the bottom of testing coupon is under tension. For FDM manufactured parts, tension and compression properties are different due to the additive manufacturing process. It is necessary to consider both compression and tension properties in simulation to accurately present the realistic flexure process. As input for the simulation, compression and tension properties were utilized while the output of flexure simulation was compared with the experimental flexure properties. In finite element model, the FDM flexure part was divided into two parts: the top part and the bottom part (Figure 5).

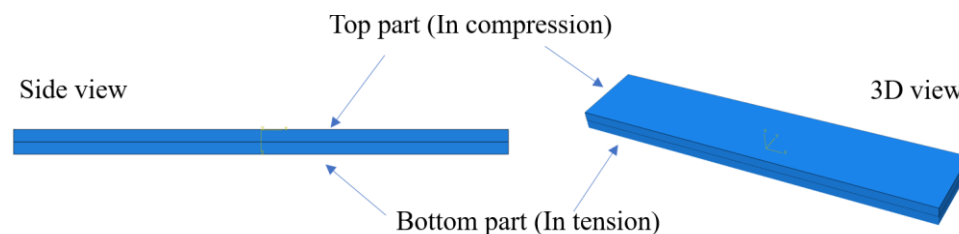


Figure 5. Modeling of flexure coupon

Both compression test results and tension test results were incorporated into finite element model to investigate the mechanical behavior of the FDM part. The compression

tests were performed using manufactured coupons (1 in. x 1 in. x 2 in.) at varying building parameters (Figure 6), and the tension tests were performed using dog bone shaped specimens (Figure 3). The test results are shown in Table 2. The experimental results including elastic and nonlinear plastic material properties were used for the material model in finite element analysis [4].

Table 2. Compression and tension properties used in finite element model

	Modulus	Yield strength
Compression	1868 MPa	82.1 MPa
Tension	1720 MPa	58.4 MPa

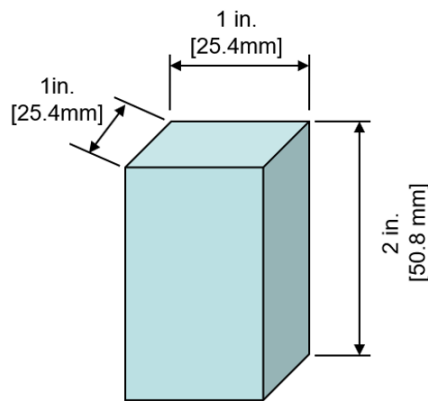


Figure 6. Coupon designs for compression tests

The assembly of FDM flexure test is shown in Figure 7. The three rod platens are modeled as rigid parts using element R3D4, and the flexure coupon is modeled as a deformable part using element C3D8R. The bottom two rod platens are fixed while the

top platen moves downward to deform the flexure coupon. During the simulation, the displacement and the reacting force of the top platen are recorded.

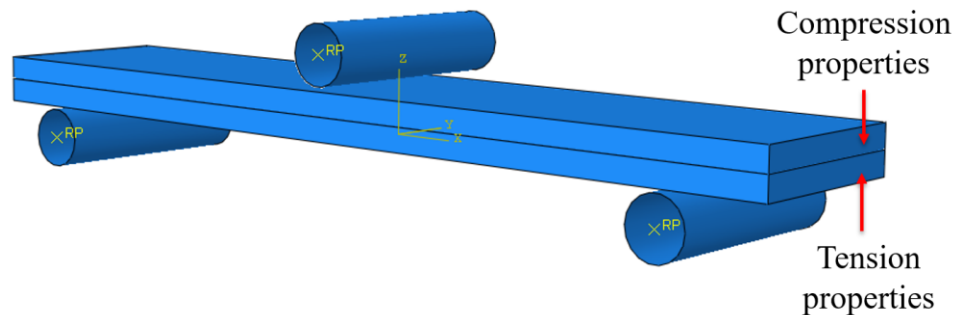


Figure 7. Simulation model for flexure test

## 4. RESULTS AND DISCUSSION

### 4.1. SOLID SAMPLE FLEXURE RESULTS FOR VARYING BUILD PARAMETERS

All flexure tests were successfully performed for the six combinations of solid flexure coupons. The modulus and yield strength results are shown in Figures 8 and 9. Overall, the XZY samples showed the highest average modulus and yield strength due to the FDM contours located and optimally positioned at the critical locations for flexure. The positioning of the contours for the XZY samples follow a pattern where the layers of each contour are oriented perpendicularly to a typical flexure crack seen during three-point bending. This means the weak interface normally seen between layers of a FDM sample was oriented perpendicularly to the tensile and compressive forces seen at the top and bottom of the FDM sample. While all modulus results were similar for each build combination, a more noticeable difference in yield strength occurred for the ZXY

samples. The ZXY samples performed the worst in yield strength due to the FDM outer contours sub-optimally positioned at the critical locations for flexure. The positioning of the contours for the ZXY samples follow a pattern where the layers of each contour are oriented parallel to typical a flexure crack formation seen during three-point bending. This means the weak interface normally seen between layers of a FDM sample was oriented such that the tensile and compressive forces directly pull and compress the weak interface between layers of the contour at top and bottom of the FDM sample. Also, in the XYZ 45°/-45° samples, the modulus and strength are less than the XZY samples because the raster angles are the primary part of the samples that resist the tension and compression during flexural loading. The raster angles are oriented off angle to the direction of tensile and compressive forces, so in the strength results, they are neither the weakest nor the strongest sample.

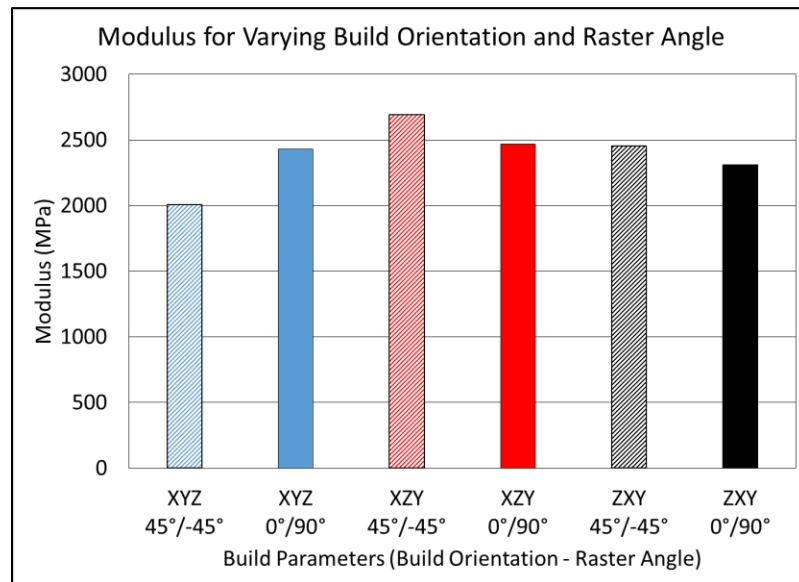


Figure 8. Ultem 1010 modulus for varying build orientation and raster angle

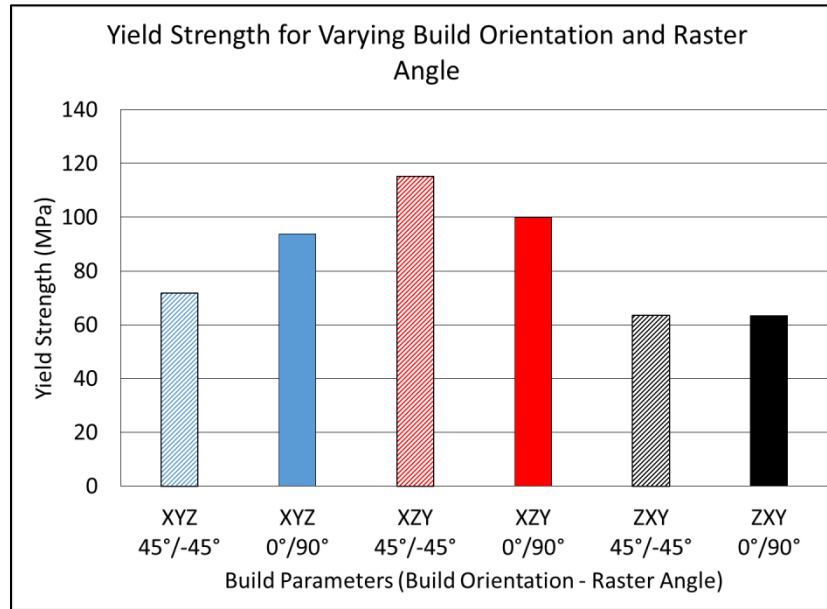


Figure 9. Ultem 1010 yield strength for varying build orientation and raster angle

A full-factorial DOE was performed with the flexure results to determine if any of the independent variables act as a main effect or interact to affect the response variable. JMP 12 statistical software package was utilized to complete the DOE. The independent variables were the build orientation and raster angle while the two response variables were the modulus and yield strength. The effects tables for both response variables are shown in Tables 3 and 4 along with the *p-value* for each main effect and interaction. For each main effect and interaction, the *p-value* indicates the probability that the null hypothesis is true. Therefore, if a *p-value* is less than 0.05, the statement can be made that the model, interaction, or main effect was significant with 95% confidence, also called the 95% significance level. For both modulus and yield strength models, the *p-values* were less than 0.0001, therefore indicating statistically significant models for the data. Upon checking the interaction (Build Orientation\*Raster Angle) of the two independent variables, the *p-values* for both modulus and yield strength were less than 0.0001,

therefore indicating that the response variables, yield strength and modulus, were affected by an interaction between the factors, build orientation and raster angle. The *p-values* for the two main effects can be ignored due to the interaction in both modulus and yield strength models.

Table 3. DOE analysis: modulus effects for different build parameters during flexure testing

Source	Degrees of Freedom	Sum of Squares	F Ratio	<i>p-value</i>
Build Orientation	2	6.92x10 <sup>5</sup>	592.63	<0.0001
Raster Angle	1	4.97x10 <sup>3</sup>	8.51	0.0075
Build Orientation * Raster Angle	2	6.52x10 <sup>5</sup>	558.51	<0.0001

Table 4. DOE analysis: yield strength effects for different build parameters during flexure testing

Source	Degrees of Freedom	Sum of Squares	F Ratio	<i>p-value</i>
Build Orientation	2	9.72x10 <sup>3</sup>	285.45	<0.0001
Raster Angle	1	46.98	2.76	0.1097
Build Orientation * Raster Angle	2	1.85x10 <sup>3</sup>	54.24	<0.0001

#### 4.2. SOLID SAMPLE FLEXURE RESULTS AT ELEVATED TEMPERATURES

Flexure tests were performed at each of the six temperatures 25, 80, 120, 150, 177, 205°C (77, 180, 250, 300, 350, 400°F) for the solid XYZ 0°/90° flexure coupons. The stress-strain results for a representative sample at each of the temperatures are shown in Figure 10. The results showed that as temperature increased the modulus and yield strength decreased (Figure 11). At 205°C, the modulus of Ultem 1010 is ~80% of the

room temperature modulus while the yield strength is ~25% of the room temperature yield strength. These flexure results are expected to be used in future studies utilizing Ultem 1010 and tooling for composite manufacturing.

#### 4.3. SPARSE SAMPLE FLEXURE RESULTS FOR SIMULATION VALIDATION

All flexure tests were successfully performed for the two air gaps for sparse flexure coupons. The modulus and yield strength results of the two sparse coupons along with the corresponding solid coupon (0.0 mm air gap) are shown in Figure 12. The modulus and yield strength showed decreasing values with increasing air gap.

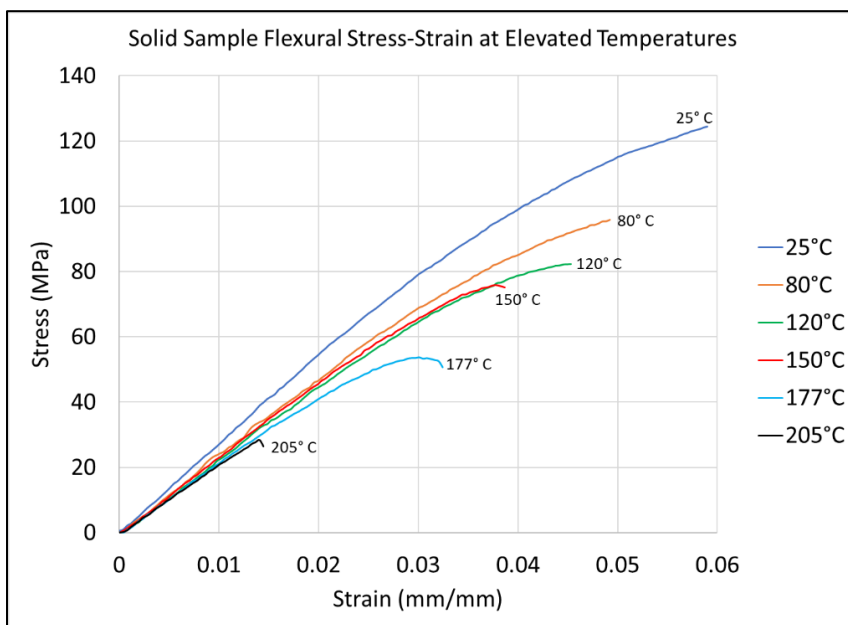


Figure 10. Elevated temperature (°C) stress-strain curves for solid flexure Ultem 1010 samples

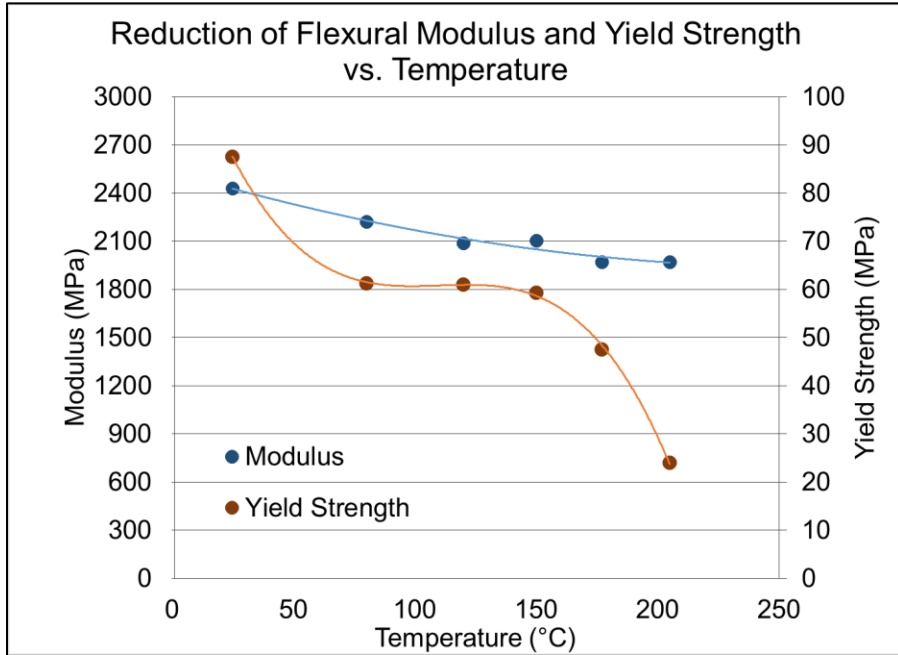


Figure 11. Reduction of modulus and yield strength with increased temperature for solid Ultem 1010 flexure samples

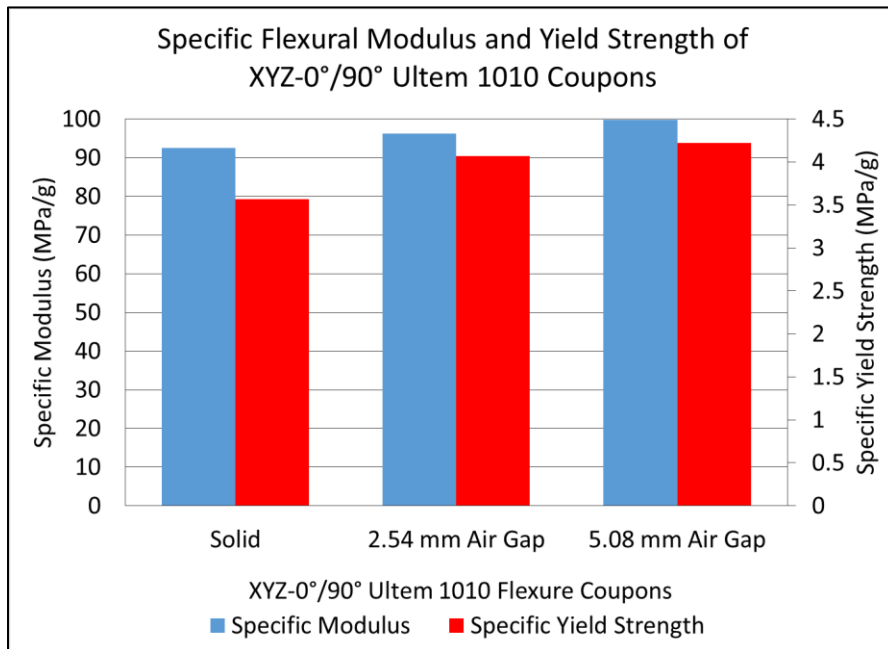


Figure 12. Flexure modulus and yield strength of XYZ 0°/90° Ultem 1010 coupons

#### 4.4. SOLID SAMPLE TENSILE TEST RESULTS

All tensile tests were successfully performed for the XYZ 0°/90° build combination. The modulus and yield strength results of the tensile coupons along with the corresponding compression data from Taylor *et al.* [4] are plotted against each other in Figure 13. The additional compression data shows compression and tension do not behave similarly (typical in many isotropic materials) due to the additive manufacturing process. The modulus and yield strength for tension and compression were measured and used as input parameters for the flexure simulation (Table 2).

#### 4.5. SIMULATION RESULTS

The developed finite element model was used to simulate flexure test of solid specimens. The build parameters are XYZ orientation and 0°/90° raster angle. Simulation results match closely with the experimental data (Figure 14). The differences between experimental and simulated results are within approximately 5%. The finite element model was verified by experimental data. The plastic strain distribution of FDM part during flexure test is plotted in Figure 15. Due to different material properties of compression and tension, the maximum plastic strain occurred at the bottom of FDM part, which is also the failure area during flexure test. Also, simulation results based on only compression properties and only tension properties were shown in Figure 14. The combined properties exhibit better agreement with experimental data.

To investigate and simulate FDM mechanical behavior, sparse FDM parts were manufactured and tested. Because the thickness of FDM specimen is relatively small, the build orientation of the sparse specimens was XYZ to demonstrate the sparse structure.

The air gaps were set as 2.54 mm and 5.08 mm, and the raster angle was chosen as 0°/90°. The respective models in finite element analysis are shown in Figure 16, with the top cap removed to show internal structure.

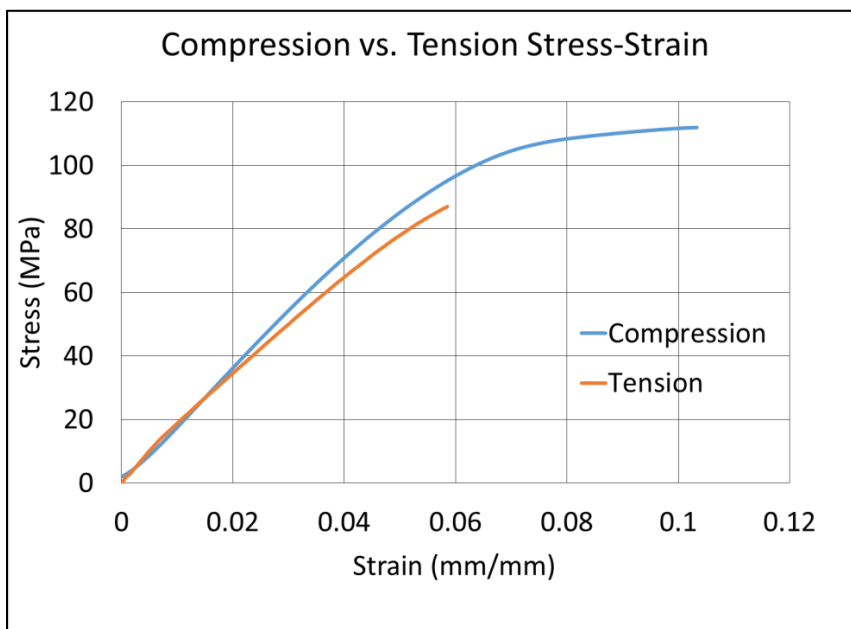


Figure 13. Compression vs. tension stress-strain results

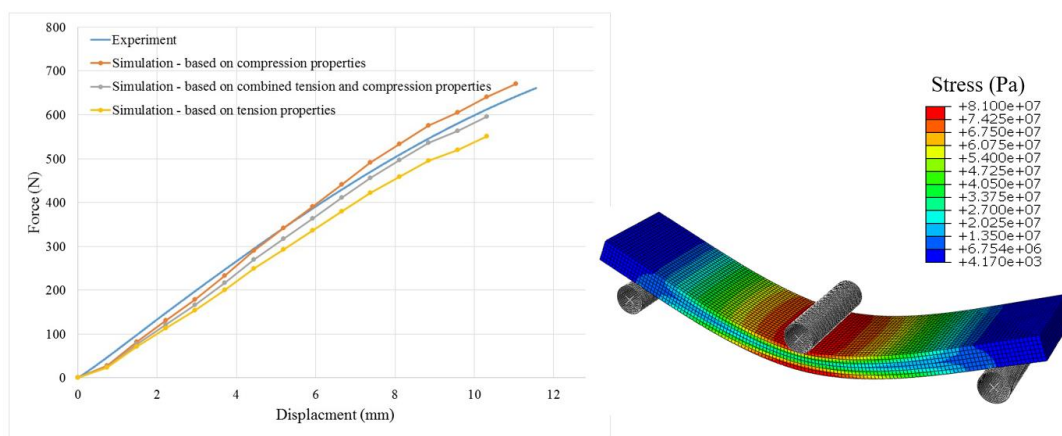


Figure 14. Comparison of solid flexure test between experiment and simulation

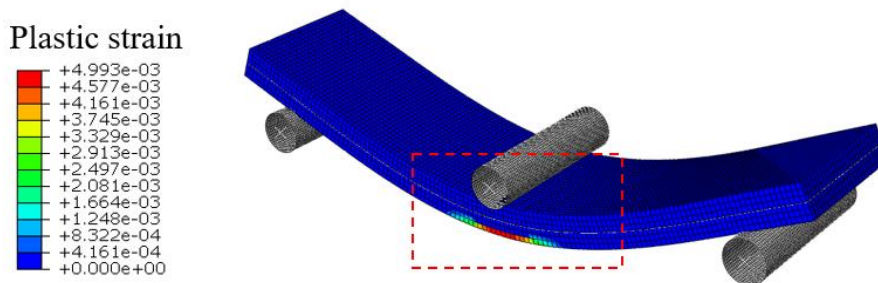


Figure 15. Plastic strain distribution of FDM part during flexure test

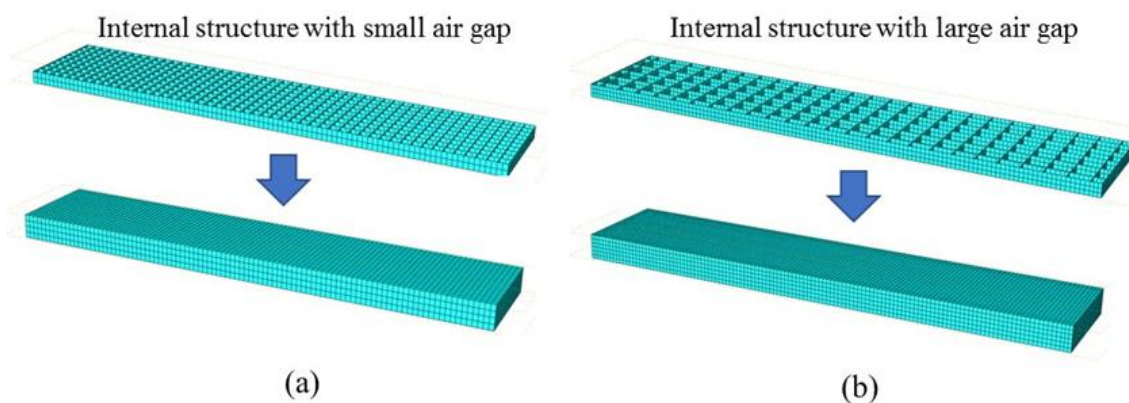


Figure 16. Modeling of sparse XYZ  $0^\circ/90^\circ$  FDM parts with: (a) 2.54 mm air gap, (b) 5.08 mm air gap

The simulation results are shown in Figures 17 and 18. Since both of these two specimens were manufactured with Ultem 1010, the maximum von Mises stress on the surface is similar under same deformation. However, since the specimen with 2.54 mm air gap has higher effective elasticity, the surface stress exhibited gradual transition from the center to the side, while the 5.08 mm air gap specimen has more discrete stress distribution on the surface.

The relative simulated displacement-load curves were compared with sparse-build coupon experimental results (Figure 17 and 18). Simulated results show good agreement

with experimental data. For 2.54 mm air gap specimen, the simulated curve is slightly larger than experimental results, and the error is within 10%. For 5.08 mm air gap, the error between experiment and simulation is reduced to 5%.

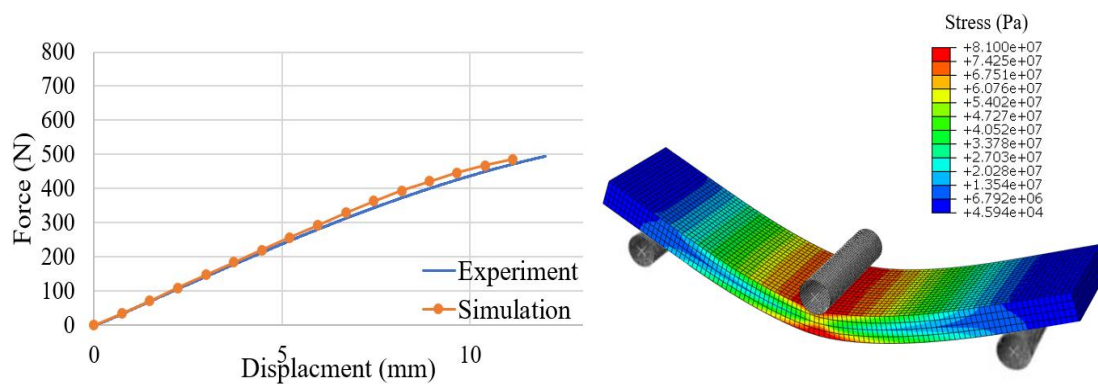


Figure 17. Stress (von Mises) distribution during flexure test (2.54 mm air gap) and comparison of sparse flexure test between experiment and simulation

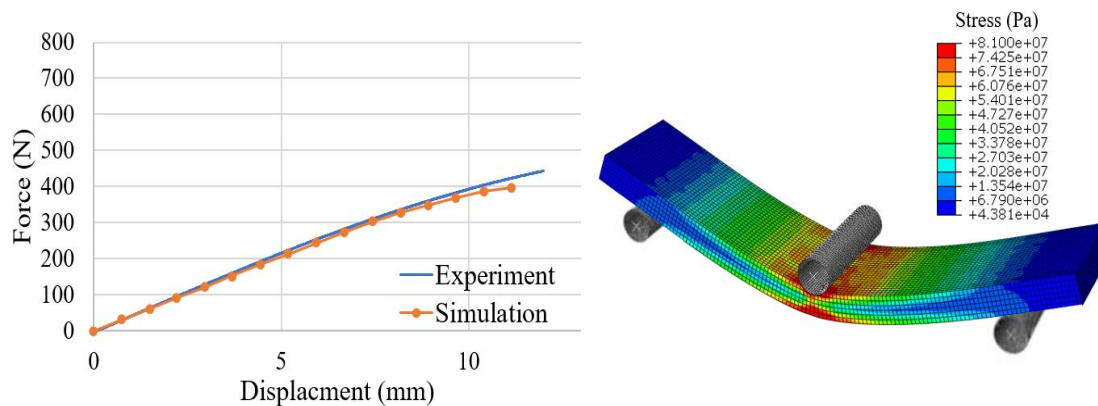


Figure 18. Stress (von Mises) distribution during flexure test (5.08 mm air gap) and comparison of sparse flexure test between experiment and simulation

## 5. CONCLUSIONS

FDM was used to manufacture Ultem 1010 coupons, and the coupons were tested for flexural properties, specifically modulus and yield strength. A full-factorial DOE was used to show the significance of the interaction of the two build parameters (build orientation and raster angle) on solid build flexure coupons. The XYZ 0°/90° build combination was chosen for elevated temperature flexure testing. For the elevated flexure testing up to 205°C (400°F), as expected, both modulus and yield strength of Ultem 1010 decreased as the testing temperature increased. Similarly to the elevated temperature tests, the XYZ 0°/90° build combination was chosen for sparse-build flexure coupons. Two different air gaps (2.54 and 5.08 mm) were tested to validate the finite element model. The model is aimed at predicting the flexure behavior of solid and sparse-build coupons. The experimental and simulation data were found to be within good agreement. These experimental and simulation results can be further extended to industrial design and manufacturing practices utilizing FDM parts produced with Ultem 1010.

## ACKNOWLEDGEMENTS

This research is sponsored by the Industrial Consortium of the Center for Aerospace Manufacturing Technologies (CAMT) at Missouri University of Science and Technology. The authors would also like to thank Michael Matlack and James Castle (Boeing) for their technical suggestions and Brett Buswell (Missouri S&T) for his help with sample fabrication.

## REFERENCES

1. Zaldivar, R.J., Witkin, D.B., McLouth, T., Patel, D.N., Schmitt, K., Nokes, J.P., "Influence of processing and orientation print effects on the mechanical and thermal behavior of 3D-Printed ULTEM® 9085 Material," *Additive Manufacturing*, Vol. 13, pp. 71-80, 2017.
2. Luzanin, O., Movrin, D., and Plancak, M., "Effect of layer thickness, deposition angle and infill on maximum flexural force in FDM built specimens," *Journal for Technology of Plasticity*, Vol. 39, pp. 49-57, 2014.
3. Motaparti, K.P., Taylor, G., Leu, M.C., Chandrashekhara, K., Castle, J., and Matlack, "Experimental investigation of effects of build parameters on flexural properties in fused deposition modelling parts," *Virtual and Physical Prototyping*, Vol. 12, No. 3, pp. 207-220, 2017.
4. Taylor, G., Wang, X., Mason, L., Leu, M.C., and Chandrashekhara, K., "Investigation of Ultem 1010 FDM sparse-build parts using design of experiments and numerical simulation," in *Proceedings of The Composites and Advanced Materials Expo*, Anaheim, CA, September 26-29, 2016.
5. Rayegani, F., and Onwubolu, G.C., "Fused deposition modelling (FDM) process parameter prediction and optimization using group method for data handling (GMDH) and differential evolution (DE)," *International Journal of Advanced Manufacturing Technology*, Vol. 73, pp. 509-519, 2014.
6. Casavola, C., Cazzato, A., Moramarco, V., and Pappalettere, C., "Orthotropic mechanical properties of fused deposition modelling parts described by classical laminate theory," *Materials & Design*, Vol. 90, pp. 453-458, 2016.
7. Li, H., Taylor, G., Bheemreddy, V., Iyibilgin, O., Leu, M. and Chandrashekhara, K., "Modeling and characterization of fused deposition modeling tooling for vacuum assisted resin transfer molding process," *Additive Manufacturing*, Vol. 7, pp. 64 - 72, 2015.
8. Torrado, A.R., Shemelya, C.M., English, J.D., Lin, Y., Wicker, R.B., and Roberson, D.A., "Characterizing the effect of additives to ABS on the mechanical property anisotropy of specimens fabricated by material extrusion 3D printing," *Additive Manufacturing*, Vol. 6, pp. 16-29, 2015.
9. Weng, Z., Wang, J., Senthil, T., and Wu, L., "Mechanical and thermal properties of ABS/montmorillonite nanocomposites for fused deposition modeling 3D printing," *Materials & Design*, Vol. 102, pp. 276-283, 2016.

10. Ji, L.B., and Zhou, T.R., "Finite element simulation of temperature field in fused deposition modeling," *Advanced Materials Research*, Vol. 97, pp. 2585-2588, 2010.
11. Górski, F., Kuczko, W., Wichniarek, R., and Hamrol, A., "Computation of mechanical properties of parts manufactured by fused deposition modeling using finite element method," In *10th International Conference on Soft Computing Models in Industrial and Environmental Applications*, Springer International Publishing, pp. 403-413, 2015.
12. Domingo-Espin, M., Puigoriol-Forcada, J. M., Garcia-Granada, A., Llumà, J., Borros, S., Reyes, G., "Mechanical property characterization and simulation of fused deposition modeling Polycarbonate parts," *Materials & Design*, Vol. 83, pp. 670-677, 2015.
13. Rezayat, H., Zhou, W., Siriruk, A., Penumadu, D., and Babu, S.S., "Structure–mechanical property relationship in fused deposition modelling," *Materials Science and Technology*, Vol. 31, pp. 895-903, 2015.
14. Garg, A., and Bhattacharya, A., "An insight to the failure of FDM parts under tensile loading: finite element analysis and experimental study," *International Journal of Mechanical Sciences*, Vol. 120, pp. 225-236, 2017.
15. Villalpando, L., Eiliat, H., and Urbanic, R.J., "An optimization approach for components built by fused deposition modeling with parametric internal structures," *Procedia CIRP*, Vol. 17, pp. 800-805, 2014.
16. Jerez-Mesa, R., Travieso-Rodriguez, J. A., Corbella, X., Busqué, R., and Gomez-Gras, G., "Finite element analysis of the thermal behavior of a RepRap 3D printer liquefier," *Mechatronics*, Vol. 36, pp. 119-126, 2016.
17. Sayre III, R., "A Comparative Finite Element Stress Analysis of Isotropic and Fusion Deposited 3D Printed Polymer," *Master Dissertation, Rensselaer Polytechnic Institute Hartford, Connecticut, USA*, 2014.
18. Liang, M., Shemelya, C., MacDonald, E., Wicker, R., and Xin, H., "3-D printed microwave patch antenna via fused deposition method and ultrasonic wire mesh embedding technique," *IEEE Antennas and Wireless Propagation Letters*, Vol. 14, pp. 1346-1349, 2015.
19. Mohamed, O. A., Masood, S. H., and Bhowmik, J. L., "Optimization of fused deposition modeling process parameters: a review of current research and future prospects," *Advances in Manufacturing*, Vol. 3, pp. 42-53, 2015.

20. ASTM D790-15 Standard Test Methods for Flexural Properties of Unreinforced and Reinforced Plastics and Electrical Insulating Materials, ASTM International, West Conshohocken, PA, 2015, <https://doi.org/10.1520/D0790-15>.
21. “Ultem 1010 Resin High-Performance Thermoplastic for Fortus 3D Production Systems: Material Specifications Sheet,” Eden Prairie, MN, 2015, [www.stratasys.com/materials/ultem-1010](http://www.stratasys.com/materials/ultem-1010).
22. ASTM D638-14 Standard Test Method for Tensile Properties of Plastics, ASTM International, West Conshohocken, PA, 2014, <https://doi.org/10.1520/D0638-14>.
23. ASTM ISO/ASTM52921-13 Standard Terminology for Additive Manufacturing-Coordinate Systems and Test Methodologies, ASTM International, West Conshohocken, PA, 2013, <https://doi.org/10.1520/ISOASTM52921-13>.

## **II. FRACTURE TOUGHNESS OF ADDITIVELY MANUFACTURED ULTEM 1010**

Gregory Taylor, Sudharshan Anandan, David Murphy, Ming Leu, and K.

Chandrashekhara

Department of Mechanical and Aerospace Engineering

Intelligent Systems Center

Missouri University of Science and Technology, Rolla, MO 65409

### **ABSTRACT**

One of the polymer additive manufacturing processes commonly used today is fused deposition modeling (FDM). FDM is the process of manufacturing three dimensional structure through the use of a layer-by-layer printing of the polymer filament. The properties of specimens manufactured using FDM are anisotropic in nature. The orientation of the rasters as well as build direction have a significant effect on damage initiation and progression. This study evaluates the fracture toughness of FDM solid-build specimens manufactured from Ultem 1010. The effects of build direction and raster orientation were investigated through the use of a full-factorial experimental design. The fracture toughness was obtained using single-edge notch bend test. The experimental design examines the effect the factors, build orientation and raster angle, have on the response, critical stress intensity factor ( $K_{I0}$ ). The primary results of this study include the relationship of the build parameters and the fracture toughness of Ultem 1010.

## 1. INTRODUCTION

Over the last decade, additive manufacturing has become a widely utilized method of manufacturing. Additive manufacturing reduces the waste common in more traditional subtractive techniques by manufacturing parts in a layer-by-layer manner. Using a three-dimensional CAD model of a proposed part additive manufacturing builds each layer and continually stacking additional layers until completion. One of the additive manufacturing processes used today is Fused Deposition Modeling (FDM). This process focuses on the extrusion of plastics through a high temperatures nozzle to manufacture the three-dimensional parts. Each layer is extruded a solidified initially on a build surface or platform and then on the preceding layer until completion. Often a support material aids in the manufacturing to structurally reinforce material that would otherwise collapse during the build process.

Additive manufacturing and FDM has become a common practice in industry today. Due to its popularity, FDM has been discussed as a possibility for manufacturing more structurally critical parts. Current research is focused primarily on tensile, compressive, and flexural behavior of additively manufactured parts. Zaldivar et al. [1] investigated the effects of build orientation on tensile properties, Poisson's ratio, and coefficient of thermal expansion of Ultem 9085. Motaparti et al. [2] observed flexural properties are dependent upon build parameters through a series of flexural tests and design of experiments. Taylor et al. [3] created a nonlinear material model through design of experiments that investigated the effect of raster angle, air gap, and wall/ cap thickness. Rayegani et al. [4] optimized process parameters for fused deposition modeling by the use of group method for data handling in order to achieve an improved

functionality of the additively manufactured part. Casavola et al. [5] used classical laminate theory typically seen in composite structures to describe the mechanical behavior of FDM parts.

While many researchers have focused tensile, compressive, and flexural behavior, other researches have been investigating the fracture toughness of FDM produced parts. Torrado et al. [6] has inserted additives into ABS material to analyze the altering of the mechanical properties. Also using SEM to aid fractography of the fracture surfaces, Xu et al. [7] has proposed a double compliance method for measuring the fracture toughness of composites which is simpler when compared to the current ASTM standard. Torres et al. [8] did tensile and fracture testing on specimens, manufactured by FDM with polylactic acid, for mechanical properties. Through design of experiments the production variables offer optimized properties depending on the tensile and fracture-type loading. Young et al. [9] applied a double cantilever beam test to compute interlayer fracture toughness for FDM manufactured unreinforced Acrylonitrile Butadiene Styrene (ABS) and chopped carbon-fiber-reinforced ABS (CF-ABS) samples. Mclouth et al. [10] found that the fracture toughness of FDM manufactured ABS was altered most significantly when the samples' print orientations were perpendicular to the respected crack plane. Song Y. et al. [11] determined that fracture toughness of PLA specimens is increased when manufactured by FDM compared to homogeneous injection moulding. Tandon et al. [12] varied the air gap of FDM coupons to find a corresponding relationship with interlaminar fracture toughness through compact tension testing. García-Guzmán et al. [13] investigated the idea of nature inspired geometric structured interfaces having positive effects on fractured properties. The study specifically tested trapezoidal interfaces.

Gardan et al. [14] presents that the FDM sample filaments direction can lead to a 30% difference in fracture toughness, concluding that the filaments directions should follow the principal direction of stress in the sample.

In the current study, the effects of build direction and raster orientation on fracture toughness were investigated through the use of a full-factorial experimental design. Single-edge notch bend tests were performed to study the conditional stress intensity factor for fracture toughness. A design of experiments examined the effect the factors, build orientation and raster angle, had on the response, conditional critical stress intensity factor ( $K_{IQ}$ ). Additionally, a microscopic evaluation of the microstructure was performed to analyze the failure mechanism of the build parameters. The primary results of this study include the relationship of the build parameters and the fracture toughness of Ultem 1010.

## **2. EXPERIMENTAL METHODOLOGY**

Methodology for this study included manufacturing of samples to testing specifications. Samples then underwent post-processing after fabrication in order to follow ASTM D5045. Testing was conducted on all samples according to the testing standards.

### **2.1. SPECIFICATIONS AND DESIGN OF EXPERIMENTS FOR FRACTURE TOUGHNESS TESTING**

Samples were fabricated according to ASTM D-5045 Standard Test Methods for Plane-Strain Fracture Toughness and Strain Energy Release Rate of Plastic Materials

[15]. The effect of build direction and raster angle on the fracture toughness was evaluated using a full-factorial design of experiments (Table 1). These two build parameters are the independent variable or factors while the response is the crack initiation fracture toughness ( $K_{IQ}$ ).

Table 1. Full-factorial design of experiments

Factors	Levels			
	A	B	C	D
Build Orientation	XYZ	XZY	-	-
Raster Angle	0°/90°	45°/-45°	All 0°	All 90°
<b>Constants</b>				
Raster Width	0.508 mm (0.02 in.)			
Contour Width	0.508 mm (0.02 in.)			
Air Gap	0 mm (0 in.)			

The  $K_{IQ}$  is considered due to the nature of additive manufactured samples and can be influenced by a combination of both material and build design. The build direction factor has two levels: XYZ and XZY [21]. The ZXY build direction was not used in the experiment due to the high likelihood of part instability during the build process. Due to the ZXY samples being build upright or tall, samples without excessive amounts of support material frequently tip over or sway during the FDM build process causing complete or partial failure for the samples. Also, since the support material is a breakaway support material, excessive amounts of support material can be difficult to

remove without damaging the part or leaving support material attached to the samples. Therefore, samples were not manufactured with the ZXY build direction. The raster angle consists factor has four levels,  $0^\circ/90^\circ$ ,  $45^\circ/-45^\circ$ , all  $0^\circ$ , and all  $90^\circ$ . This angle is measured from the x-axis on the x-y build plane. In total, 40 total samples were manufactured for the eight build combinations with five replications each.

For the parameters, the build orientation is the direction the part is printed within the FDM machine build space. For a typical FDM machine, the x-axis runs parallel to the front of the machine, the y-axis runs perpendicular to the x-axis from machine front to machine back, the z-axis runs perpendicular to x-axis and y-axis as well as normal to the layers of the parts. All raster angles are measured as the angle between the internal wall and the x-axis. Constant build parameters include: raster width (0.508 mm), contour width (0.508 mm), and air gap (0 mm). Finished samples for both orientations are shown below in Figure 1.

## **2.2. FABRICATION OF ULTEM 1010 SPECIMENS WITH THE FDM PROCESS**

The fracture toughness samples were fabricated with Ultem 1010 using the Stratasys Fortus 400mc machine at Missouri University of Science and Technology. The procedure for the fabrication of the FDM parts involves the following:

1. Pre-processing: A three-dimensional models of the coupons were created in CAD software (SOLIDWORKS 2017) with overall dimensions of 88 mm x 20 mm x 10 mm. The model was exported as a Stereo Lithography (STL) file to Stratasys Insight 9.1 software. The Insight software creates the build

toolpath for each of the build orientations and specifies the build parameters for the FDM coupons. An STL file is created for each build combination and provided to the FDM machine for fabrication of the fracture toughness coupons.

2. Fabrication: The Fortus 400mc machine fabricated the FDM coupons for each build combination through the extrusion of Ultem 1010 filament via a heated nozzle in a layer-by-layer manner.
3. Post-processing: After fabrication, the support material was mechanically removed from the coupons.

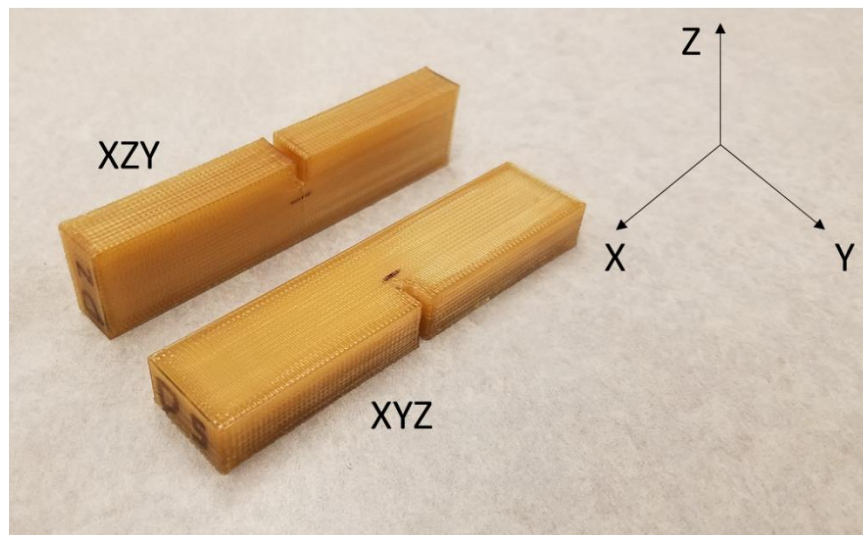


Figure 1. Build orientation

### 2.3. FRACTURE TOUGHNESS TESTING PROCEDURE

Fracture toughness tests were conducted according to the guidelines in ASTM 5045. The single edge notch bend (SENB) configuration was selected in this study. Specimens were manufactured with width of 20 mm, thickness of 10 mm, and a length of

88 mm (Figure 2). A notch was pre-built into the specimen geometry with crack added after manufacturing.

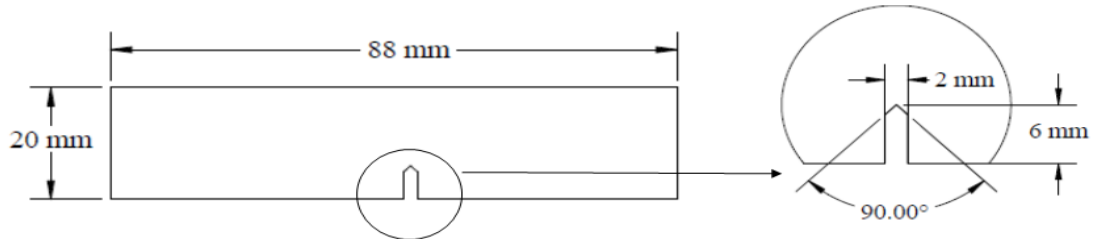


Figure 2. Specimen dimensions for fracture toughness test

A crack needs to be cut onto the specimen before testing. The required crack length for the specimen dimensions chosen in this study is 9-13 mm calculated according to Equation 1.

$$B, a, (W - a) > 2.5 \left( \frac{K_{IQ}}{\sigma_y} \right)^2 \quad (1)$$

where  $a$  is initial crack length,  $W$  is specimen width and  $B$  is specimen thickness.  $K_{IQ}$  in this equation is an estimate of fracture toughness which was obtained by preliminary testing.  $\sigma_y$  is the yield strength of additively manufactured Ultem 1010 [15].

The crack was extended using a jeweler's saw, to a length of ~11mm. The initial crack length for each sample was measured using a pair of calipers with a least count of 0.01 mm before testing. The specimen was loaded using a three-point bending test fixture with a loading span of 80 mm as shown in Figure 3.

Specimens were loaded until failure at a rate of 0.05 in/minute. Using the maximum load required to propagate the crack, the crack initiation fracture toughness or  $K_{IQ}$  was calculated according to equation 2.

$$K_{IQ} = \frac{P_m f\left(\frac{a}{W}\right)}{B(W)^{\frac{1}{2}}} \quad (2)$$

where  $P_m$  is the load required for crack propagation,  $a$  is initial crack length,  $W$  is specimen width and  $B$  is specimen thickness. The term,  $f\left(\frac{a}{W}\right)$  is a calibration factor, defined in Equation 3:

$$f(x) = 6x^{\frac{1}{2}} \left[ \frac{1.99 - x(1-x)(2.15 - 3.93x + 2.7x^2)}{(1+2x)(1-x)^{\frac{3}{2}}} \right] \quad (3)$$

where  $x$  stands for  $\frac{a}{W}$ .

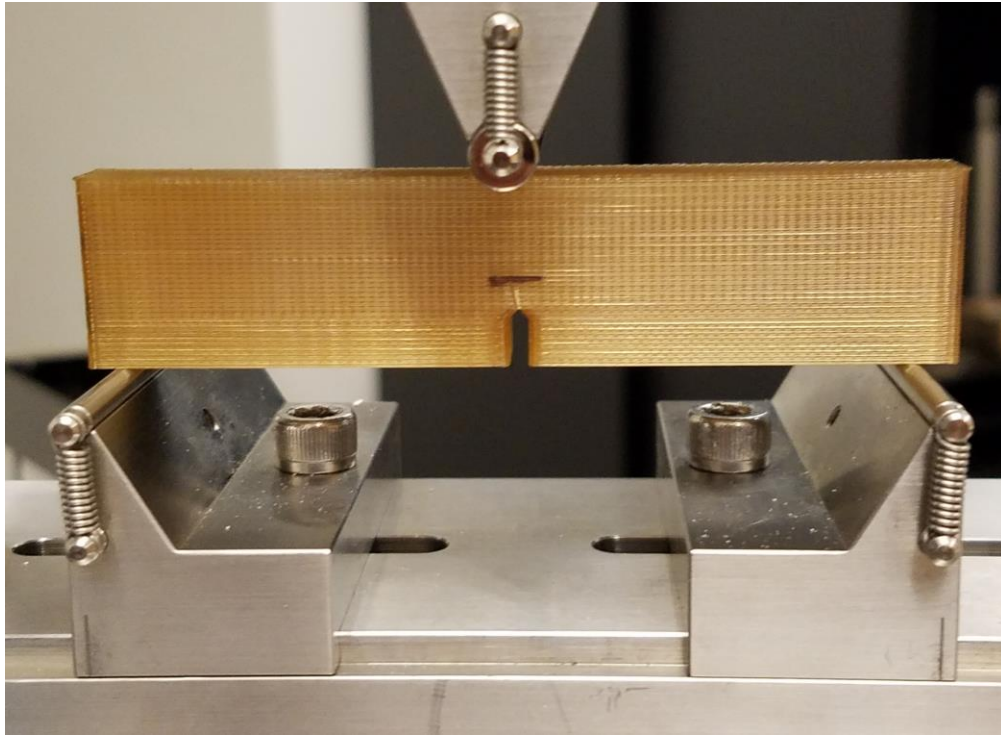


Figure 3. Test setup for the SENB fracture toughness test

### 3. RESULTS AND DISCUSSION

#### 3.1. FRACTURE TOUGHNESS RESULTS

All fracture toughness tests were successfully performed for 40 samples and the yield stress of every sample was found. A majority of samples fully fractured into two pieces while several samples held together slightly beyond the onset of fracture (Figure 4). From the yield stress, the  $K_{I0}$  was calculated from Equation 2 for each sample and tabulated into average results show in Figure 5.

From the results shown in Figure 5, the highest critical stress intensity factor for any sample occurred for the XZY build orientation and all  $0^\circ$  raster angle. This result is expected due to the build layers oriented normal to the intended propagation of the crack during fracture, thus increasing the fracture toughness. In both XYZ and XZY build orientations, the results demonstrated similar trends across each raster angle.

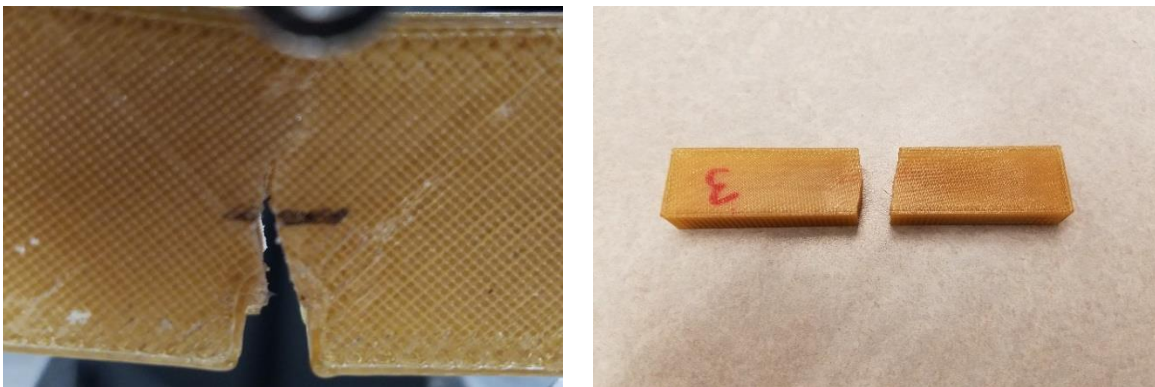


Figure 4. (a) Partial fracture of an Ultem 1010 sample, (b) Complete fracture of an Ultem 1010 sample

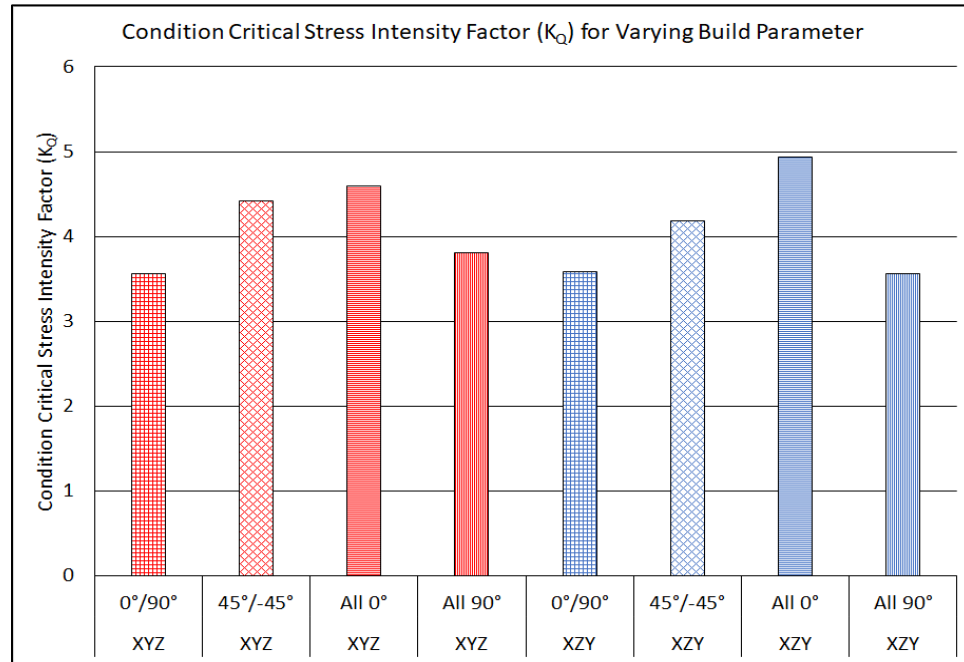


Figure 5. Average KI<sub>Q</sub> of varying build orientation and raster angles for Ultem 1010 samples

### 3.2. DESIGN OF EXPERIMENTS RESULTS

A full-factorial design of experiments was performed with the SENB results to determine if the response variable, KI<sub>Q</sub>, is being significantly affected by any of the independent variables, build orientation and raster angle. To determine the significance, the p-value must be less than 0.05, or in other words, the model, interaction, or main effect is significant with 95% confidence. The DOE was analyzed with JMP 12 statistical software, and the results are shown in Tables 2 & 3. From the analysis of variance (ANOVA) shown in Table 2, the model was found to be significant (p-value less than 0.0001), and therefore, the response, KI<sub>Q</sub>, changes with one or more variables or combinations of variables. From the effects table (Table 3), the interaction (Build Orientation\*Raster Angle) between the build orientation and raster angle was looked at

for significance, however the combination of the two variables did not show significance with the p-value greater than 0.05. Finally, the two main effects, build orientation and raster angle, were evaluated and only the raster angle showed to be significant with p-value less than 0.05. This indicates that for the testing performed, only the raster angle affected the differentiation of  $K_{IQ}$  between samples. Examining Figure 5, the trend of  $K_{IQ}$  for both XYZ and XZY build orientations is similar for the same raster angles, but different raster angles indeed show different  $K_{IQ}$  results.

### 3.3. MICROSTRUCTURE EVALUATION

The results of fracture toughness testing indicate that samples manufactured using all  $0^\circ$  raster angle have the best fracture toughness values. The fracture toughness of a sample with all  $0^\circ$  raster angle and XYZ build direction is shown in Figure 6(a). The rasters are oriented perpendicular to the direction of crack propagation. Under continued loading, failure occurs due to failure of individual filaments in the specimen. Specimens manufactured with all  $90^\circ$  build direction have the least fracture toughness (Figure 6(b)). The failure in these specimens is solely in the interlayer bond region. In FDM structures, the interlayer bond is the weakest region and therefore fracture toughness is lowest in samples manufactured with rasters oriented along the direction of crack propagation. Failure in samples manufactured with  $0^\circ/90^\circ$  raster angle is a combination of the above-mentioned failure modes (Figure 7(a)). Even though these samples have some layers oriented perpendicular to the direction of crack propagation, it did not result in any significant increase in fracture toughness. Figure 7(b) shows the failure propagation in samples with  $45^\circ/-45^\circ$  raster angle. Failure occurs mainly due to intra-layer failure,

similar to 0° build direction specimens, but inter-layer failure is also observed. While the fracture toughness of these samples is lower than the all 0° raster angle specimens, it is much higher than the specimens manufactured using all 90° build direction.

Table 2. Analysis of variance

Source	DF	Sum of Squares	Mean Square	F Ratio
Model	7	8.307468	1.18678	9.4651
Error	27	3.385388	0.12538	<b>p-value</b>
C. Total	34	11.692856	-	<.0001

Table 3. Build parameter effects table

Source	Nparm	DF	Sum of Squares	F Ratio	p-value
Raster Angle	3	3	7.9488281	21.1318	<.0001
Build Orientation	1	1	0.0093882	0.0749	0.7864
Raster Angle*Build Orientation	3	3	0.5200095	1.3824	0.2694

For practical applications, samples manufactured using all 0° or 90° build directions can exhibit orthotropic properties, with reduced mechanical strength along the direction perpendicular to the rasters. Previous works have demonstrated that tensile and flexural strength of FDM manufactured specimens also follows a similar trend. To obtain a good combination of mechanical strength and fracture toughness, a 45°/-45° build

direction may be recommended, where the rasters are oriented at  $45^\circ$  to the expected direction of crack propagation.



Figure 6. (a) Samples with all  $0^\circ$  rasters, (b) Samples with all  $90^\circ$  rasters



Figure 7. (a) Samples with  $0^\circ/90^\circ$  rasters, (b) Samples with  $45^\circ/-45^\circ$  rasters

#### 4. CONCLUSIONS

The Ultem 1010 fracture toughness coupons with varying build orientation and raster angle were manufactured with fused deposition modeling. The samples were tested for conditional critical stress intensity factor using single-edge notch bend test. A full-factorial design of experiments was conducted, and the interaction between build orientation and raster angle did not significantly affect the conditional critical stress intensity factor. Further, only the raster angle, not build direction, showed significance for affecting the conditional critical stress intensity factor. The microstructures of the samples were evaluated to determine the causes of the failure. Samples failed due to failure of the either individual filaments, interlayer bonding, intra-layer bonding, or combination of failure methods.

#### ACKNOWLEDGEMENTS

The authors would like to thank Leah Mason, Missouri University of Science and Technology, for her effort in manufacturing the samples.

#### REFERENCES

1. Zaldivar, R.J., Witkin, D.B., McLouth, T., Patel, D.N., Schmitt, K., and Nokes, J.P., "Influence of processing and orientation print effects on the mechanical and thermal behavior of 3D-Printed ULTEM® 9085 Material," *Additive Manufacturing*, Vol. 13, pp. 71-80, 2017.
2. Motaparti, K.P., Taylor, G., Leu, M.C., Chandrashekhara, K., Castle, J., and Matlack, M., "Experimental investigation of effects of build parameters on flexural properties in fused deposition modelling parts," *Virtual and Physical Prototyping*, Vol. 12, No. 3, pp. 207-220, 2017.

3. Taylor, G., Wang, X., Mason, L., Leu, M.C., and Chandrashekhara, K., "Investigation of Ultem 1010 FDM sparse-build parts using design of experiments and numerical simulation," in Proceedings of The Composites and Advanced Materials Expo, Anaheim, CA, September 26-29, 2016.
4. Rayegani, F. and Onwubolu, G.C., "Fused deposition modeling (FDM) process parameter prediction and optimization using group method for data handling (GMDH) and differential evolution (DE)," *International Journal of Advanced Manufacturing Technology*, Vol. 73, pp. 509-519, 2014.
5. Casavola, C., Cazzato, A., Moramarco, V., and Pappalettere, C., "Orthotropic mechanical properties of fused deposition modelling parts described by classical laminate theory," *Materials & Design*, Vol. 90, pp. 453-458, 2016.
6. Torrado, A.R., Shemelya, C.M., English, J.D., Lin, Y., Wicker, R.B., and Roberson, D.A., "Characterizing the effect of additives to ABS on the mechanical property anisotropy of specimens fabricated by material extrusion 3D printing," *Additive Manufacturing*, Vol. 6, pp. 16-29, 2015.
7. Xu, W. and Guo, Z.Z. "A simple method for determining the mode I interlaminar fracture toughness of composite without measuring the growing crack length," *Engineering Fracture Mechanics*, Vol. 191, pp. 476-485, 2018.
8. Torres, J., Cole, M., Owji, A., DeMastry, Z., and Gordon, A.P., "An approach for mechanical property optimization of fused deposition modeling with polylactic acid via design of experiments," *Rapid Prototyping Journal*, Vol. 22 (2), pp. 387-404, 2016.
9. Young, D., Kessler, J., and Czabaj, M., "Interlayer fracture toughness of additively manufactured unreinforced and carbon-fiber-reinforced acrylonitrile butadiene styrene," *Proceedings of the American Society for Composites - 31st Technical Conference*, ASC 2016.
10. McLouth, T.D., Severino, J.V., Adams, P.M., Patel, D.N., and Zaldivar, R.J., "The impact of print orientation and raster pattern on fracture toughness in additively manufactured ABS" *Additive Manufacturing*, Vol. 18, pp. 103-109, 2017.
11. Song, Y., Li, Y., Song, W., Yee, K., Lee, K.-Y., and Tagarielli, V.L., "Measurements of the mechanical response of unidirectional 3D-printed PLA," *Materials and Design*, Vol. 123, pp. 154-164, 2017.
12. Tandon, G.P., Whitney, T.J., Gerzeski, R., Koerner, H., and Baur, J., "Process parameter effects on interlaminar fracture toughness of FDM printed coupons," *Conference Proceedings of the Society for Experimental Mechanics Series*, Vol. 7, pp. 63-71, 2017.

13. García-Guzmán, L., Távara, L., Reinoso, J., Justo, J., and París, F., “Fracture resistance of 3D printed adhesively bonded DCB composite specimens using structured interfaces: Experimental and theoretical study,” *Composite Structures*, Vol. 188, pp. 173-184, 2018.
14. Gardan, J., Makke, A., and Recho, N., “Improving the fracture toughness of 3D printed thermoplastic polymers by fused deposition modeling,” *International Journal of Fracture*, Vol. 210 (1-2), pp. 1-15, 2018.
15. ASTM D5045-14, Standard Test Methods for Plane-Strain Fracture Toughness and Strain Energy Release Rate of Plastic Materials, ASTM International, West Conshohocken, PA, 2014, [www.astm.org](http://www.astm.org).

### **III. MECHANICAL AND OPTICAL BEHAVIOR OF A CONTINUOUS GLASS FIBER-REINFORCED TRANSPARENT COMPOSITE**

Gregory Taylor, David Murphy, T. Schuman, and K. Chandrashekhara

Department of Mechanical and Aerospace Engineering

Missouri University of Science and Technology, Rolla, MO 65409

#### **ABSTRACT**

In this study, a continuous glass fiber-reinforced composite is manufactured using the vacuum assisted resin transfer molding (VARTM) process. The composite is manufactured from an S-glass fiber acting as reinforcement and an epoxy resin as matrix. Unlike a traditional E-glass fiber reinforcement, S-glass fibers give higher stiffness and provide easier manufacturability due to the value of the refractive index of S-glass. The epoxy resin is synthesized Epon 826, Epalloy 5200, and Hexahydrophthalic Anhydride and tailored to match refractive indices of the glass fibers. After synthesis of the resin, composite panels are manufactured from the resin and fiber using VARTM. Composite panels are visually inspected for transparency and mechanical testing is performed. Both tension and flexure is performed on the manufactured composites panels.

#### **1. INTRODUCTION**

The most common transparent material utilized today is glass. While glass can be used for its hardness, strength, chemical resistance, and abrasion resistance, its primary disadvantages are the catastrophic or brittle nature exhibited upon failure and the weight of a pure glass material. Composites offer a lighter and often stronger alternative to glass

and similar materials for applications in which weight of material can greatly impact the performance of a structure. However, composites are traditionally heterogeneous, and therefore are difficult to make transparent. The idea of manufacturing a transparent composite relies heavily on matching and maintaining the refractive index match between both the fiber and the matrix [1, 2]. The applications of an optically clear composite include ballistic armor, strengthened windows for vehicles, aircraft, or buildings, and visors for eyewear [3, 4].

Recently researches have approached transparent composites in several different ways, but the main driving force for successful manufacturing of a transparent composite is for armor applications. Strassburger *et. al* [5] studied projectile impact on several types of transparent armor materials currently in use. Sun *et. al* [6] modeled different projectile impacts on various transparent armor systems. While maintaining the goal of transparent armor, several researchers have been investigating thermoplastic polymers rather than thermoset polymers. Stenzler and Goulbourne [7] investigated the impact properties of PMMA and PC multilayered composite laminates. A more common topic in transparent composites is transparent nanocomposites. Nanocomposites benefit from increased transparency when compared to short fiber or continuous fiber composites. Retegi *et. al* [8] created an all-renewable resource transparent nanocomposite using epoxidized soybean oil and bacterial cellulose nanofibers. Rai and Singh [9] combined both thermoplastic and nanocomposite materials through the manufacture and evaluation of the impact behavior of the composite panels.

However, the ideal goal of transparent composite is to manufacture a continuous fiber composite to maximize the possible structural properties. Krug *et. al* [10]

manufactured a high-performance composite using a UV cure for a epoxy-resin system and S-glass fibers. Results showed high strength due to the S-glass, but transparency became an issue with yellow and blue dispersion occurring on final samples. M. Velez *et. al* manufactured transparent panels as well but utilized a special rectangular cross-section fiber to reduce dispersion in the composite panels. Additionally, a finite element model was developed to study the impact behavior of the transparent panels.

In the current study, a continuous fiber-reinforced transparent composite is manufactured from S-glass woven fibers and specially tailored resin with matching refractive index. The S-glass woven fabric is selected due to the high strength of fibers, high impact resistance of the weave, and better refractive index matching with the epoxy resin system. The resin system is composed of several commercially available epoxies that cure to match the refractive index of the fibers. Composite panels are manufactured with VARTM, and the panels are tested for both tensile and flexural properties following ASTM standards.

## **2. MATERIALS**

### **2.1. FIBER REINFORCEMENT SELECTION**

An S-glass woven fabric manufactured by BGF Industries is used as the fiber reinforcement in the transparent composites. The reinforcement consists of a bi-directional 0°/90° 8-Harness Satin weave. The fabric has a weight of 303.5 g/m<sup>2</sup> (8.95 oz/yd<sup>2</sup>) and thickness of 0.23 mm (0.009) in. The refractive index of the fibers is reported by BGF Industries to be approximately 1.522 (Table 1).

Table 1. Refractive indices of fiber and resin

<b>Materials</b>	<b>Manufacturer</b>	<b>Refractive Index</b>
Epon 826	Momentive	1.573
Epalloy 5200	Emerald	1.486
HHPA	Dixie	1.47
S-Glass	Owens Corning	1.522

## 2.2. EPOXY SELECTION AND SYNTHESIS

To synthesize a compatible resin with matching refractive index equal to the fiber refractive index, a resin system needs to consist of at least two parts to tailor a refractive index based on the volume of each of the constituents. In order to maintain a stoichiometric balance between both epoxy and cure hardener, a second epoxy is introduced. The two epoxies chosen for the resin system are Epon 826 from Momentive Performance Materials and Epalloy 5200 from Emerald Performance Materials. The cure hardener selected for the resin system is Hexahydrophthalic anhydride (HHPA) from Dixie Chemical. The refractive index of the liquid epoxies and cure hardener are shown in Table 1. A transparent catalyst is also utilized to initiate the chain growth but is ignored in terms of refractive index due the minimal amount of catalyst needed compared to other constituents.

The synthesis of the resin consisted of varying the amount of the two epoxies to modify the refractive index of the resulting resin. All samples are composed of a constant amount of HHPA and catalyst. The HHPA is held constant according to a 1:1 stoichiometric balance between total epoxy and cure hardener. The total amount of epoxy was varied between 100% Epon 826 and 100% Epalloy 5200. Resins are manufactured with these epoxy ratios and narrowed incrementally until a refractive index was matched

with the S-glass fibers. The refractive index is matched to the S-glass fibers by curing a small amount of a resin formulation and S-glass fibers in aluminum pans. The cure cycle of the resin system is a 110°C cure for one hour and is further discussed in Section 3. Upon curing, the aluminum pans are peeled, and the resulting sample (Figure 1) is visually inspected for matching refractive index. The resulting resin system is shown in Table 2. For the masses listed in Table 2, the volume of the resulting resin system is approximately 15 mL, but the total ratio of the constituents can be scaled to a desired volume of resin system.



Figure 1. Resin system test sample with S-glass fibers

Table 2. Resin system

<b>Materials</b>	<b>Refractive Index</b>	<b>Mass (g)</b>
Epon 826	1.573	2.523
Epalloy 5200	1.486	7.000
HHPA	1.47	8.500
Catalyst	Unknown	0.090
<b>Resin System</b>	<b>~ 1.522 (Cured)</b>	<b>18.113</b>

### 3. MANUFACTURING

To manufacture the transparent composites from the S-glass fibers and epoxy resin system, the vacuum assisted resin transfer molding process (VARTM) was selected due to the ease of manufacture of the composite panels. The process is similar to a typical autoclave process in which the composite is manufactured under a sealed vacuum bag for the given cure cycle. The major difference of the two processes is lack of a pressurized atmosphere for the VARTM process. The VARTM process operates entirely at atmosphere pressure (101 kPa).

The manufacture of the transparent composites utilizes a two part mold consisting of a large glass mirror (60 cm x 60 cm) for the base support and a small glass square (18 cm x 18 cm x 0.64 cm) for the upper mold. The glass mirror and glass square are selected due to their polished surface finish. The transparency of a panel is greatly influenced by the surface quality, and therefore, molds with a polished surface provide the best opportunity for composite transparency. Before manufacturing, the surfaces of both molds are cleaned and prepared with the application of a two part release agent. The release agent consists of Chemlease 15 Sealer EZ and Chemlease® PMR-90 EZ from Chem Trend.

After preparation of the molds, four layers of the S-glass woven fabric are laid up in between the two molds as shown in Figure 2. Sealant tapes are positioned around the edges of the glass mirror mold and vacuum tube inlet and outlet are positioned on either side of the fiber layup. The glass square mold is placed directly on the fibers, and the glass mirror mold is prepared for infusion (Figure 3). A vacuum bag is applied, and a vacuum is connected to the layup before the infusion to check for any leaks in the layup.

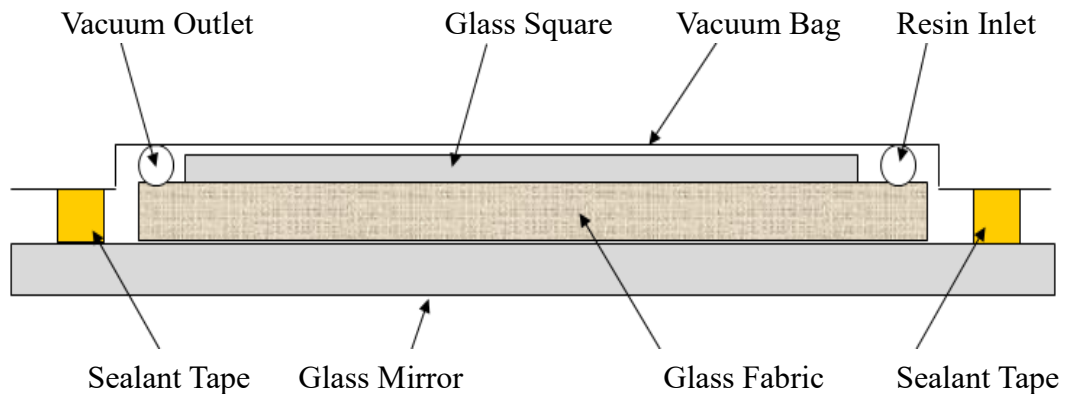


Figure 2. VARTM process schematic for transparent composites

The infusion process for VARTM consists of applying vacuum to the mold and heating both layup and epoxy resin to 50°C. Once the resin system has fully reached 50°C, the inlet line is opened to the epoxy resin to allow flow into the layup. Throughout the entirety of the infusion, both the layup and resin are maintained at 50°C to keep a low resin viscosity. With the resin open to the atmosphere, the resin is pushed through the layup which is under vacuum. The resin flows from the inlet into the fibers and across the mold towards the outlet. Once the resin has fully infused the part, the inlet and outlet are sealed to prevent any air from entering the layup. The layup is then placed under the resin

cure cycle of 110°C for one hour (Figure 4). After curing, the transparent panel is examined for visible voids, microscopic voids, surface finish, and refractive index matching. If the sample contained few or no visible (non-microscopic) voids, the sample was cut and prepared for additional testing.

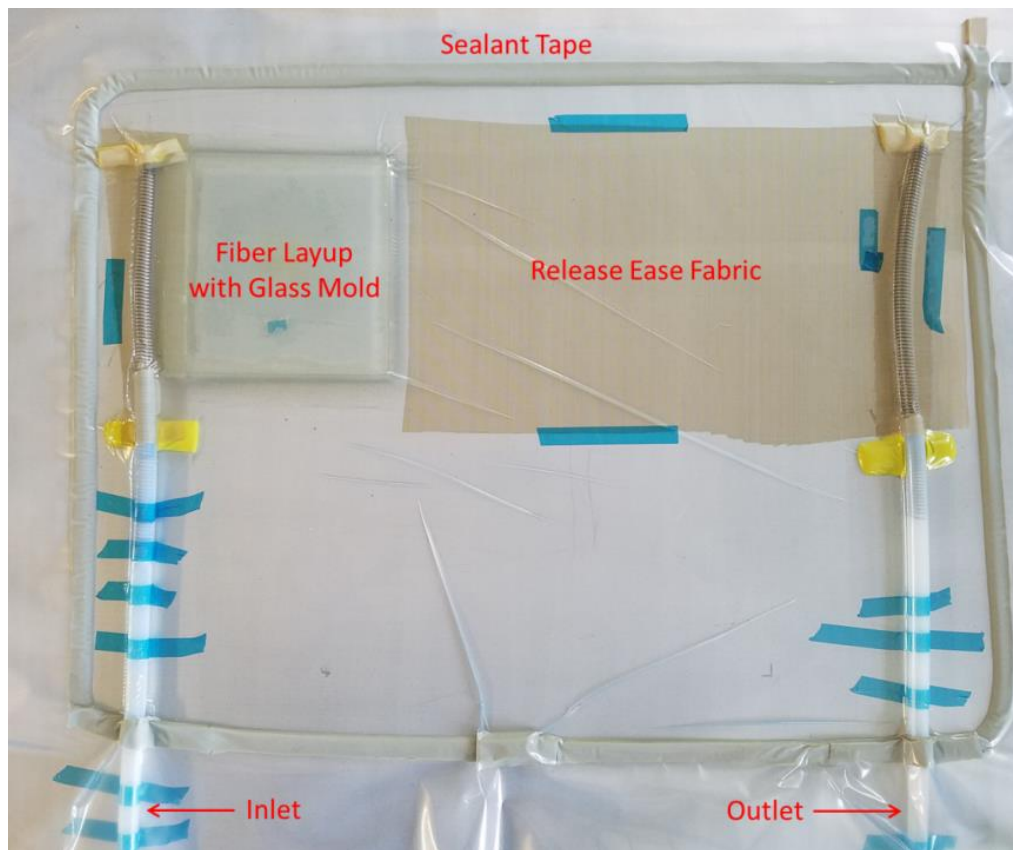


Figure 3. VARTM layup before infusion

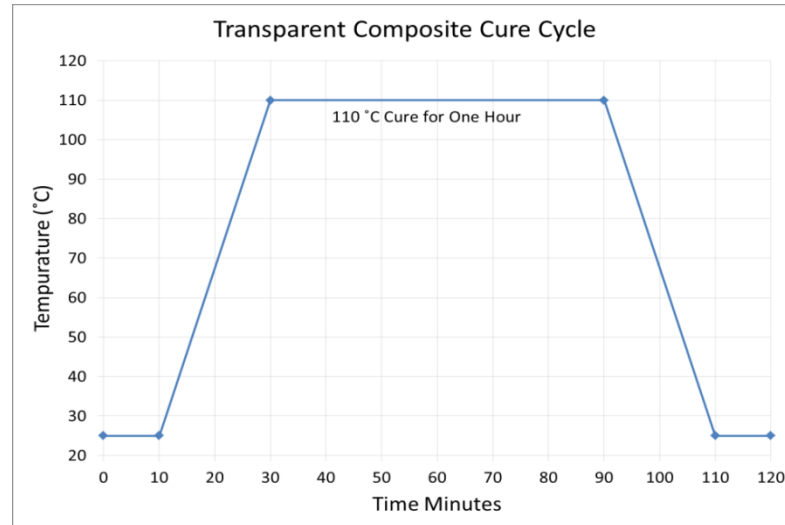


Figure 4. Transparent composite cure cycle

## 4. EXPERIMENTAL METHODOLOGY

### 4.1. TENSION TEST SPECIFICATIONS

All tension tests were conducted according to ASTM D3039– 17 Standard Test Method for Tensile Properties of Polymer Matrix Composite Materials [12]. Five samples are cut to approximate dimensions of 152.4 mm x 12.7 mm x 1.14 mm (6 in. x 0.5 in. x 0.045 in.). Precise dimensions for each sample are recorded before each test. For the video extensometer, the gauge length is marked as two black dots approximately 1 in. apart on all samples (Figure 5). The tensions tests are conducted on an Instron 5985 universal testing machine. Load and deflection are recorded along with strain from the video extensometer. Stress is determined after testing from load and sample dimensions.



Figure 5. Tension test setup for transparent composites

#### 4.2. FLEXURE TEST SPECIFICATION

All flexure tests were conducted according to ASTM D7264– 15 Standard Test Method for Flexural Properties of Polymer Matrix Composite Materials [13]. The four-point bend test is used due to heterogeneous materials composing the composite. Four samples are cut to dimensions of 152.4 mm x 12.7 mm x 1.52 mm (6 in. x 0.5 in. x 0.06 in.). In accordance with ASTM D7264, samples are chosen to be tested with a 60:1 span-to-thickness ratio due to the thickness of the transparent panels, and each have a span of 91.44 mm (3.6 in.). The test speed is 1 mm/min calculated as

$$R = \frac{ZL^2}{6d} \quad (1)$$

where R is test speed in mm/min, Z is rate of straining of the outer fiber (provided as 0.01 mm/mm/min), L is the span in mm, and d is the width of the beam in mm. The test setup is shown in Figure 6.

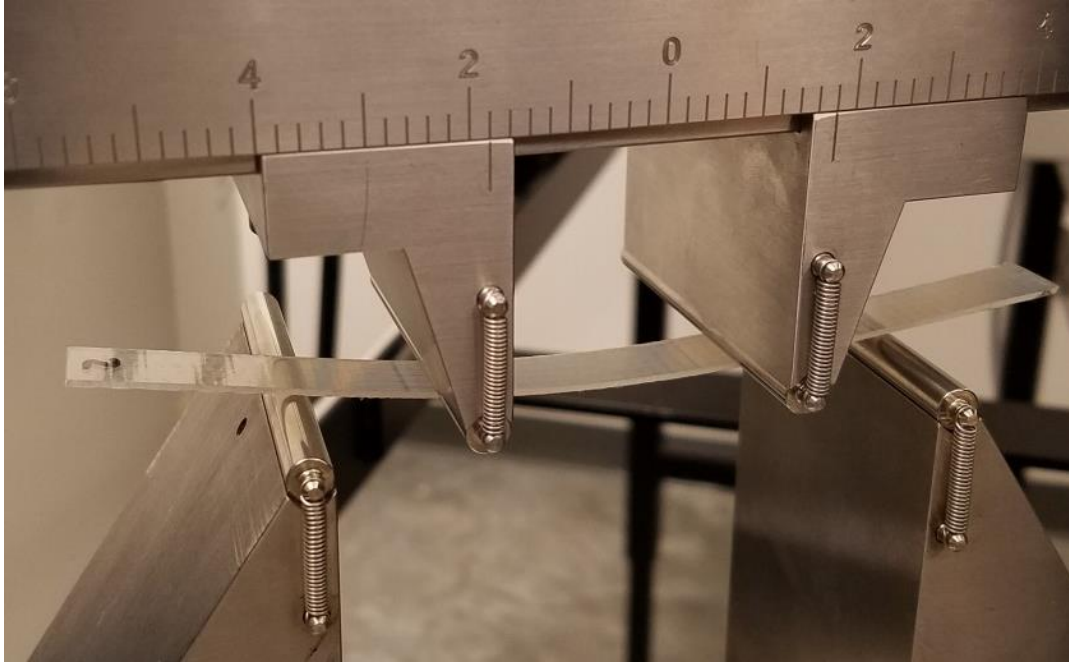


Figure 6. Four-point flexure test setup for transparent composites

## 5. RESULTS

### 5.1. TENSION TEST RESULTS

All five tension samples were successfully tested. Of the five samples, four broke within the gauge section, and the fifth sample's tensile modulus and strength were within the standard deviation of other four samples. The tensile samples had a tensile modulus of  $17.86 \pm 1.32$  GPa and tensile strength of  $624.6 \pm 32.8$  MPa. The tensile stress-strain curves for the transparent composite samples are shown in Figure 7.

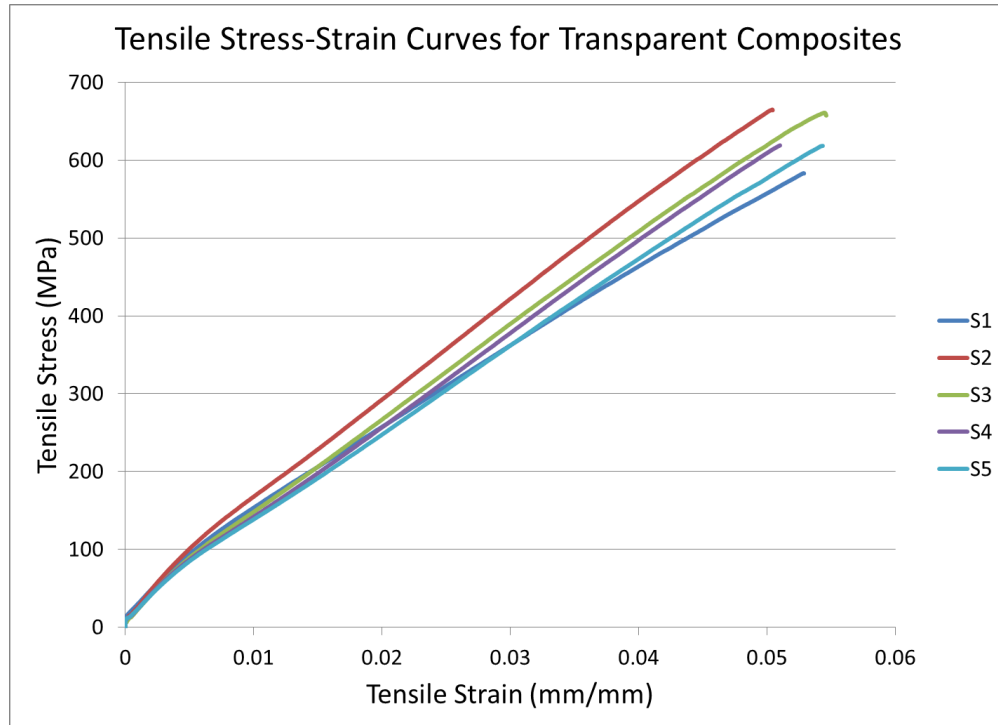


Figure 7. Tensile stress-strain curves for the transparent composite

## 5.2. FLEXURE TEST RESULTS

All four flexure samples were successfully tested. The four samples did not fail, but the tests stopped due to the stagnation of the flexure stress with increasing strain. The flexural samples had a flexural modulus of  $19.69 \pm 1.23$  GPa and flexural strength of  $155.7 \pm 3.8$  MPa. The flexural stress-strain curves for the transparent composite samples are shown in Figure 8. Due to a low load (40 N) on a 10kN load cell, the samples experienced some fluctuation in the values of flexural stress near the yield point. However, the results show a consistent value for both flexural modulus and strength.

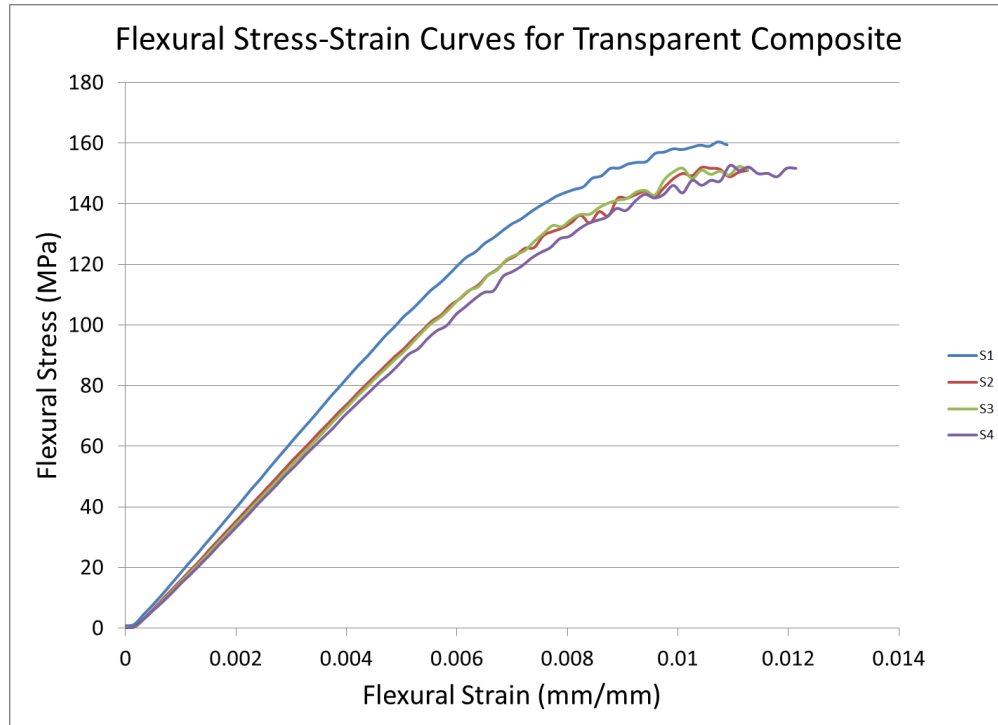


Figure 8. Flexural stress-strain curves for the transparent composite

## 6. CONCLUSIONS

An epoxy resin system was synthesized from two epoxy polymers, Epon 826 and Epalloy 5200, and cure hardener, HHPA. The resulting resin system was tailored to match the refractive index of an S-glass woven fabric upon cure. Transparent composite panels were manufactured by infusing the epoxy resin into an S-glass continuous fiber VARTM layup. The VARTM layups were then cure at a cure cycle of 110°C cure for one hour. After cure, samples were examined for visual transparency. The panels were tested for both tensile and flexural properties. The resulting tensile modulus was 17.86 +/- 1.32 GPa, and the tensile strength was found to be 624.6 +/- 32.8 MPa. The resulting flexural modulus was 19.69 +/- 1.23 GPa, and the flexural strength determined to be 155.7 +/- 3.8 MPa.

## REFERENCES

1. F. Gibson, "A review of recent research on mechanics of multifunctional composite materials and structures," *Composite Structures*, Vol. 92, no. 12, pp. 2793-2810, 2010.
2. V. Menta, R. Vuppalapati, K. Chandrashekhara and T. Schuman, "Manufacturing of transparent composites using vacuum assisted resin transfer molding process," *Polymer and Polymer Composites*, Vol. 22, No. 9, pp. 843-849, 2014.
3. M. Grujicic, W. C. Bell, and B. Pandurangan, "Design and material selection guidelines and strategies for transparent armor systems," *Materials and Design*, Vol. 34, pp. 808-812, 2012.
4. P. G. Dehmer and M. A. Klusewitz, "High Performance Visors," Army Research Laboratory, Technical Report No. ARL-RP-45, 2002.
5. E. Strassburger, M. Hunzinger, J. W. McCauley, and P. Patel, "Experimental methods for characterization and evaluation of transparent armor materials," *Ceramic Engineering and Science Proceedings*, Vol. 31, No. 5, 2010.
6. X. Sun, C. Lai, T. Gorsich, and D. W. Templeton, "Optimizing Transparent Armor Design Subject To Projectile Impact Conditions," *Ceramic Engineering and Science Proceedings*, Vol. 29, No. 6, pp. 15-22, 2009.
7. J. Stenzler and N. Goulbourne, "Impact mechanics of transparent multi-layered polymer composites," *Proceedings of the 2009 SEM 2009 Annual Conference & Exposition on Experimental & Applied Mechanics*, Vol. 3, pp. 1963-1982, 2009.
8. A. Retegi, I. Algar, L. Martin, F. Altuna, P. Stefani, R. Zuluaga, P. Gañán, I. Mondragon, "Sustainable optically transparent composites based on epoxidized soybean oil (ESO) matrix and high contents of bacterial cellulose (BC)," *Cellulose*, Vol. 19, pp. 103-109, 2012.
9. K. Rai and D. Singh, "Impact resistance behavior of polymer nanocomposite transparent panels," *Journal of Composite Materials*, Vol. 43, No. 2, pp. 139-151, 2009.
10. D. Krug III, M. Ascuncion, V. Popova and R. Laine, "Transparent fiber glass reinforced composites," *Composites Science and Technology*, Vol. 77, pp. 95-100, 2013.
11. M. Velez, W. Braisted, G. Frank, D. Day and M. Mclaughlin, "Impact strength of optically transparent glass ribbon composites," *Journal of composite materials*, Vol. 46, No. 14, pp. 1677-1695, 2012.

12. ASTM D3039 / D3039M-17, Standard Test Method for Tensile Properties of Polymer Matrix Composite Materials, ASTM International, West Conshohocken, PA, 2017, [www.astm.org](http://www.astm.org).
13. ASTM D7264 / D7264M-15, Standard Test Method for Flexural Properties of Polymer Matrix Composite Materials, ASTM International, West Conshohocken, PA, 2015, [www.astm.org](http://www.astm.org).

## SECTION

### 3. CONCLUSIONS

Ultem 1010 coupons were manufactured by the FDM process for testing of the flexural modulus and yield strength. To understand the effects of the FDM build parameters on the coupons, a full-factorial DOE was utilized to show the two build parameters, build orientation and raster angle, interact to affect the flexural modulus and yield strength of solid-build coupons. Elevated temperature testing was performed on the XYZ 0°/90° build combination up to 205°C. As the temperature was increased from room temperature up to 205°C, the flexural modulus and strength both decreased. Sparse-build coupons were tested at varying air gap to validate the finite element model. With gradual improvement, the model's goal is to eventually be able to predict the behavior of both the solid-build and sparse-build coupons. Experimental and simulation data were found to be in good agreement with each other.

Similarly to the flexure testing, Ultem 1010 were tested for fracture toughness using a DOE. The Ultem 1010 coupons were built with varying build orientation and raster angle to investigate the fracture toughness response. The condition critical stress intensity factor ( $K_{I0}$ ) was recorded for the single-edge notch bend test. Through the full-factorial DOE, the interaction between build orientation and raster angle did not significantly contribute to a change in the conditional critical stress intensity factor. From the DOE, the only main effect that significantly contributed to the change in conditional critical stress intensity factor was the raster angle. An examination of the results indicated that for the two build directions tested, neither had an effect on  $K_{I0}$ . A microstructures

evaluation was conducted to determine the causes of the failure for the different raster angles. The all 0° raster angle samples failed due to individual filament failure. The all 90° raster angle samples failed from interlayer bonding failure. The 0°/90° raster angles failed from a combined filament and interlayer bonding failure. The 45°/-45° raster angle samples failed to intra-layer bonding.

For transparent composites, a resin system was synthesized from Epon 826, Epalloy 5200, and HHPA. The resin system's cured refractive index matched the refractive index of the S-glass woven fabric chosen for the composites. Transparent composite panels were manufactured from the continuous fibers and matching epoxy resin system. The cure cycle used for this VARTM process was a one hour cure at 110 °C. The cured composites were visually inspected for transparency and further tested for tension and flexure. From the testing, it was found that tensile modulus was 17.86 +/- 1.32 GPa, tensile strength was 624.6 +/- 32.8 MPa, flexural modulus was 19.69 +/- 1.23, GPa, and flexural strength was 155.7 +/- 3.8 MPa.

## VITA

Gregory Taylor was born in Belleville, Illinois. He received his Bachelor of Science in Aerospace Engineering in 2012 from Missouri University of Science and Technology in Rolla, Missouri. He continued at Missouri University of Science and Technology and enrolled in the M.S. degree program in Aerospace Engineering. After receiving his Master of Science in December 2014, he enrolled in the Ph.D. program at Missouri University of Science and Technology. During his time in both the master's and Ph.D. program from 2012 to 2018, he held the positions of both Graduate Research Assistant and Graduate Teaching Assistant in the Department of Mechanical and Aerospace Engineering. In December 2018, he received his Ph.D. in Aerospace Engineering from Missouri University of Science and Technology.